J. Fluid Mech. (1979), *vol.* 92, *part* 2, *pp.* 269–301
Printed in Great Britain

The distortion of turbulence by a circular cylinder

By R. E. BRITTER, J. C. R. HUNT†
Department of Applied Mathematics and Theoretical Physics,
University of Cambridge
AND J. C. MUMFORD
Cavendish Laboratory, University of Cambridge

(Received 12 September 1977 and in revised form 28 June 1978)

The flow of grid-generated turbulence past a circular cylinder is investigated using hot-wire anemometry over a Reynolds number range from $4{\cdot}25 \times 10^3$ to $2{\cdot}74 \times 10^4$ and a range of intensities from 0·025 to 0·062. Measurements of the mean velocity distribution, and r.m.s. intensities and spectral energy densities of the turbulent velocity fluctuations are presented for various radial and circumferential positions relative to the cylinder, and for ratios of the cylinder radius a to the scale of the incident turbulence L_x ranging from 0·05 to 1·42. The influence of upstream conditions on the flow in the cylinder wake and its associated induced velocity fluctuations is discussed.

For all measurements, detailed comparison is made with the theoretical predictions of Hunt (1973). We conclude the following.

(i) The amplification and reduction of the three components of turbulence (which occur in different senses for the different components) can be explained qualitatively in terms of the *distortion* by the mean flow of the turbulent vorticity and the 'blocking' or 'source' effect caused by turbulence impinging on the cylinder surface. The relative importance of the first effect over the second increases as a/L_x increases or the distance from the cylinder surface increases.

(ii) Over certain ranges of the variables involved, the measurements are in quantitative agreement with the predictions of the asymptotic theory when $a/L_x \ll 1$, $a/L_x \gg 1$ or $|\mathbf{k}|a \gg 1$ (where $\mathbf{k}$ is the wavenumber).

(iii) The incident turbulence affects the gross properties of the flow in the cylinder wake, but the associated velocity fluctuations are probably statistically independent of those in the incident flow.

(iv) The dissipation of turbulent energy is *greater* in the straining flow near the cylinder than in the approach flow. Some estimates for this effect are proposed.

1. Introduction

The fluid mechanics of turbulence impinging on a bluff obstacle has a number of interesting aspects:

(i) the distortion of the turbulence by the mean flow, the distortions becoming very large near the surface;

(ii) the interaction of the turbulence with the rigid surface of the obstacle;

† Also Department of Engineering.

0022-1120/79/4189-6400 $02.00

(iii) the effects of the turbulence on the obstacle's boundary layer and its position of separation;

(iv) the interaction of the turbulence with the unsteady separated flows in the wake.

Some of these aspects are common to other turbulent flows. The first two are found when a jet impinges normally on a surface, a special feature of this flow being that the mean flow is rotational and the turbulence intensity very high (Gutmark, Wolfshtein & Wygnanski 1978). The second is present when turbulence impinges on a thin plate or a moving wall downstream of a grid (Hunt & Graham 1977). The first aspect also occurs in the familiar distortion of turbulence in contractions (see Townsend 1976). The unique feature of the turbulence around a bluff body is the simultaneous presence of all four.

This paper presents measurements of the turbulence around a circular cylinder, with particular emphasis on the distortion of turbulence from its upstream form, as a function of the ratio of the scale of the incident turbulence (L_x) to the radius of the cylinder (a). Previous detailed studies of the distortion around bluff bodies have concentrated on the stagnation line and have been restricted to a limited range of a/L_x (Sadeh, Sutera & Maeder 1970; Bearman 1972; Petty 1972). Detailed comparisons are made throughout this paper between the measurements and the theoretical predictions of Hunt (1973, hereafter referred to as H). These are briefly reviewed in § 2. The measurements of the distribution of mean velocity and angles of separation of the flow from the cylinder are presented in § 4, and in § 5 the properties of the turbulence are described.

The practical applications of this study to pressure fluctuations on bluff bodies and to turbulent diffusion from sources near bluff bodies have been described elsewhere (Hunt 1976; Britter, Hunt & Puttock 1976).

2. Theoretical considerations

Consider the flow of weak, and nominally homogeneous, isotropic turbulence around a circular cylinder at high Reynolds number, i.e.

$$u'_\infty \ll \overline{U}_\infty, \quad u'_\infty L_x/\nu \gg 1, \quad \overline{U}_\infty a/\nu \gg 1,$$

where u'_∞ and $\overline{U}_\infty$ are the upstream root-mean-square streamwise turbulent and mean velocities, a is the cylinder radius, L_x is the integral scale of the turbulence and ν is the kinematic viscosity. It is instructive to define the three flow regions depicted in figure 1: the wake region W, the boundary layers on the cylinder B and the external flow region E.

In a non-turbulent steady incident flow the wake flow is unsteady and induces a weak, fluctuating, irrotational velocity $u^{(w)}$ in the external region E. When the incident flow is turbulent, the problem arises of whether these self-induced velocity fluctuations in E are significantly modified and, in particular, whether there is an appreciable correlation between $u^{(w)}$ and the velocity fluctuations $u^{(T)}$ in the incident turbulence.

The spatial extent δ of the boundary layer is small compared with the cylinder radius and if we now impose the restriction that $\delta \ll L_x$, then the boundary layer can

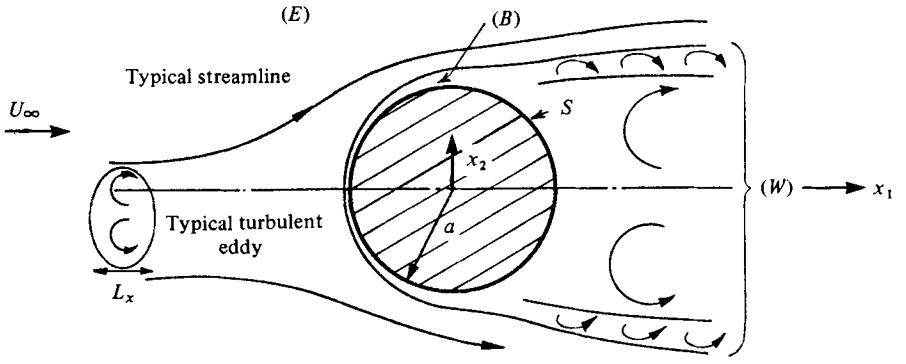

FIGURE 1. The regions of flow near a bluff body and the relevant length scales of the body and of the incident turbulence (from Hunt 1973).

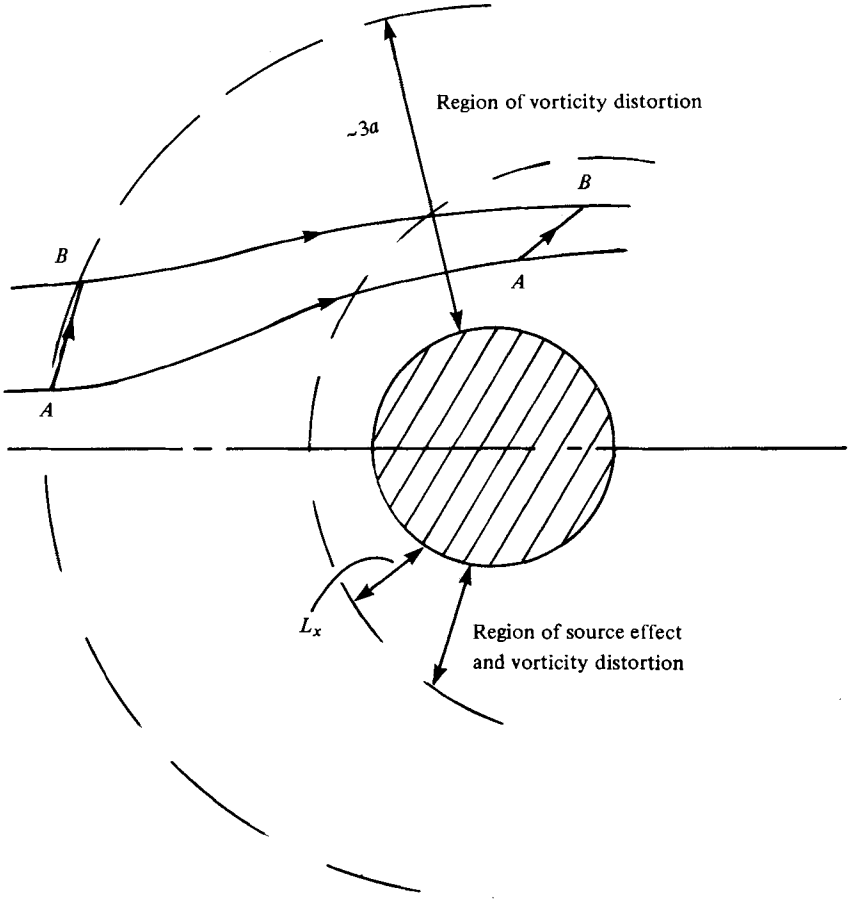

FIGURE 2. The regions of vorticity distortion and source effect for flow near a bluff body. Note the stretching and rotation of the vortex line element AB.

be neglected (in its direct effect on the external flow region E). Thus, for the moment, neglecting the boundary layer and ignoring the weak irrotational velocity fluctuations $u^{(w)}$ induced by the wake, the turbulence in the region E will be distorted by the mean velocity field, distorted by the imposition of boundary conditions (no flow through the cylinder surface), and will be subject to the normal turbulent–turbulent interactions and energy dissipation processes.

If, in addition, the time scale L_x/u'_∞ for the nonlinear interactions between energy-containing eddies (the 'turnover' time) is large compared with the time $a/\overline{U}_\infty$ required for fluid to flow round the obstacle, i.e. $(u'_\infty/\overline{U}_\infty)(a/L_x) \ll 1$, then the turbulence is primarily distorted by the mean velocity field before it can be modified significantly by nonlinear interactions, i.e. it is subjected to a 'rapid distortion'.

With these assumptions the movement of vortex elements will be described by the movement of line elements and, with a known field of mean velocity, the movement of line elements is also known. The field of mean velocity will stretch and rotate vortex lines (see figure 2), altering the distribution of turbulent vorticity and thus changing the turbulent velocities. This stretching and rotating of vortex lines will take place over the distance in which the mean velocity field is significantly altered by the bluff body, i.e. over a distance a few times the radius of the cylinder a.

The boundary condition that there should be no flow across the surface of the body gives rise to a 'blocking' distortion of the turbulence by the body or a distribution of imaginary sources on the body. This effect produces a change in the turbulence over a distance comparable to the scale of turbulence L_x or the cylinder radius a, whichever is smaller.

In summary, when the ratio a/L_x is *small* the blocking mechanism will be dominant and extend to a distance approximately L_x from the cylinder; however when a/L_x is *large* the vorticity distortion is the dominant process out to a distance approximately $3a$ from the cylinder except that, within a distance L_x from the body, blocking will be comparable to vorticity distortion (see figure 2). One objective of this paper is to quantify the terms 'small' and 'large', which the asymptotic results of H did not.

The previous arguments can be applied to the various wavenumber components in the turbulence. For example, the three-dimensional spectrum of the longitudinal component of turbulence on the stagnation line, when a/L_x is such that there is little variation in intensity as the cylinder is approached, should be attenuated at low wavenumbers and amplified at higher wavenumbers.

3. Experimental apparatus

Experimental work was carried out in a $0{\cdot}45 \times 0{\cdot}45$ m wind tunnel in the Department of Applied Mathematics and Theoretical Physics, University of Cambridge. The mean and turbulent velocities were uniform over $0{\cdot}4 \times 0{\cdot}4$ m. With the aim of producing a wide range of a/L_x, planar square grids with various mesh sizes M ($1{\cdot}143 \times 10^{-1}$ m, $5{\cdot}08 \times 10^{-2}$ m and $2{\cdot}54 \times 10^{-2}$ m) and bar-to-mesh ratio 1:4 were placed after the 4:1 contraction at the entrance to the working section. These grids produced approximately homogeneous isotropic turbulence with the range of integral scales and intensities summarized in Table 1 at downstream distances x_1 from the grids corresponding to the cylinder locations used for most of the measurements reported in the following sections. The integral scales L_x were evaluated as the product of the

M (m)	x_1/M	$u_1'/\overline{U}_1$	u_2'/u_1'	u_3'/u_1'	L_x (m)
0·114	15·6	0·062	0·84	0·85	0·060
0·0508	20	0·051	0·78	0·85	0·032
0·0254	40	0·025	0·88	0·88	0·015
0·0254	15	0·050	0·88	0·88	0·011
No grid	—	0·001	—	—	> 0·08

TABLE 1

mean velocity $\overline{U}_\infty$ and the integral time scales† τ of the longitudinal velocity component. The intensity ratios of the turbulence components are also given in Table 1.

All experiments were carried out at an incident velocity of 10 m/s, which, with cylinder radii of $3{\cdot}18 \times 10^{-3}$ m, $6{\cdot}35 \times 10^{-3}$ m and $2{\cdot}06 \times 10^{-2}$ m, gave cylinder Reynolds numbers of $4{\cdot}25 \times 10^3$, $8{\cdot}5 \times 10^3$ and $2{\cdot}74 \times 10^4$. The measurements have not been corrected for the effect of wind-tunnel blockage.

The vertical cylinders were rigidly fixed to the tunnel walls; for a few measurements a splitter plate on the x_1 axis of length $4a$ was used. Disa constant-temperature anemometers (type 55D01) and linearizers (type 55D10) were used. The single-wire probes were of type 55P03 with the wire parallel to the axis of the cylinder. The X-wire probes were of type 55P52. The probe holders were attached to the end of a 6 mm diameter stainless-steel rod which extended through a streamwise slot in the top of the wind tunnel. The slot was sealed using two 'wind-up' steel tape-measures. Outside the tunnel, the rod was clamped to a vertical traverse which was attached to a streamwise traverse which was in turn attached to the top plate of the tunnel. Movement in the third (transverse) direction was obtained by moving the entire top-plate assembly transversely relative to the remainder of the tunnel working section. The probe positions relative to the cylinder were determined to an accuracy of 0·25 mm.

The probe holder was introduced parallel to the axis of the cylinder for all measurements other than the measurement of the axial velocity fluctuations on the stagnation line, for which it was introduced laterally. The mean velocity and turbulence intensity measurements were taken on-line, and the fluctuating velocity signals were recorded on a Tandberg F.M. tape recorder with a frequency response of 0–2·5 kHz. These signals were later digitized and recorded on magnetic tape using the PACE–ICL 1400 hybrid computer system of the University of Cambridge Control Engineering Group. The digital tape was analysed on the University of Cambridge IBM 370/165 to evaluate the probability density, autocorrelation and spectral energy density functions of the velocity signals.

The decay of the u_1 component of turbulence behind the grids could be fitted by either of the expressions

$$(u_1'/\overline{U}_\infty)^{-2} \propto (x_1 - X_0) \quad \text{(see Batchelor 1960)}, \tag{3.1}$$

$$(u_1'/\overline{U}_\infty)^{-2} \propto (x_1 - X_1)^{1{\cdot}25} \quad \text{(see Comte-Bellot \& Corrsin 1971)}, \tag{3.2}$$

X_0 and X_1 being chosen for the best fit with the data ($X_0/M = 5{\cdot}5$, $X_1/M = 3{\cdot}0$).

† Using $R(t)$ to denote the autocorrelation function of the longitudinal velocity component, τ was taken to be

$$\int_0^{t_0} R(t)\, dt,$$

where t_0 is the smallest value of t satisfying $R(t) = 0$. For a discussion of the arbitrariness and errors in this procedure see Comte-Bellot & Corrsin (1971, appendix D).

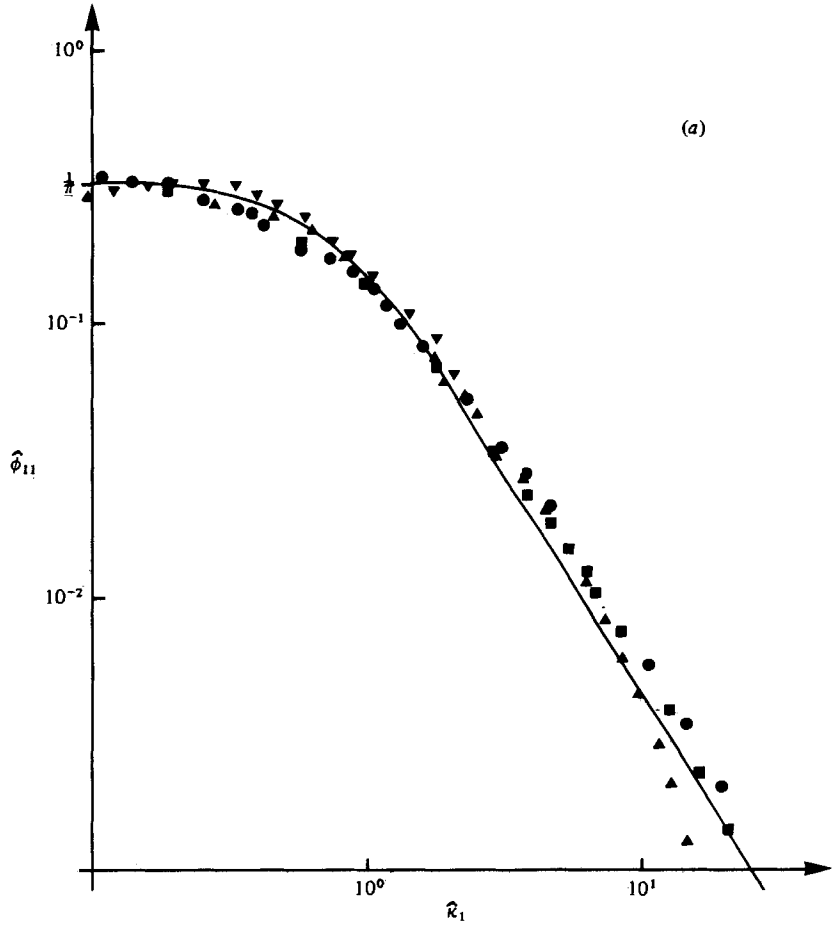

FIGURE 3 (a). For legend see next page.

The measured spectra of the longitudinal velocity fluctuations behind the grids may be approximated by the von Kármán expression (Bearman 1972)

$$\hat{\phi}_{11}(\hat{\kappa}_1) = \pi^{-1}\{1+(1{\cdot}34\hat{\kappa}_1)^2\}^{-\frac{1}{6}}, \tag{3.3}$$

where

$$\hat{\phi}_{11}(\hat{\kappa}_1) = \phi_{11}(n)\,\overline{U}_\infty/4\pi u'^2_{1\infty}\,L_x$$

and

$$\hat{\kappa}_1 = \kappa_1^* L_x = 2\pi n L_x/\overline{U}_\infty, \tag{3.4}$$

as shown in figure 3(a).

The spectra of the lateral velocity fluctuations (figure 3b) do not show good agreement with the formula derived from (3.3) by assuming isotropy, namely

$$\phi_{22,33}(\hat{\kappa}_1) = \frac{1}{2\pi}\,\frac{\{1+(2{\cdot}19\hat{\kappa}_1)^2\}}{\{1+(1{\cdot}34\hat{\kappa}_1)^2\}^{\frac{11}{6}}}. \tag{3.5}\dagger$$

Defining L_{x2} as the integral scale deduced from the lateral velocity spectra as $\hat{\kappa}_1 \to 0$, it is apparent that L_{x2}/L_x is an increasing function of the ratio of tunnel width to

† This differs from equation (6.8) of H, which contains a misprint.

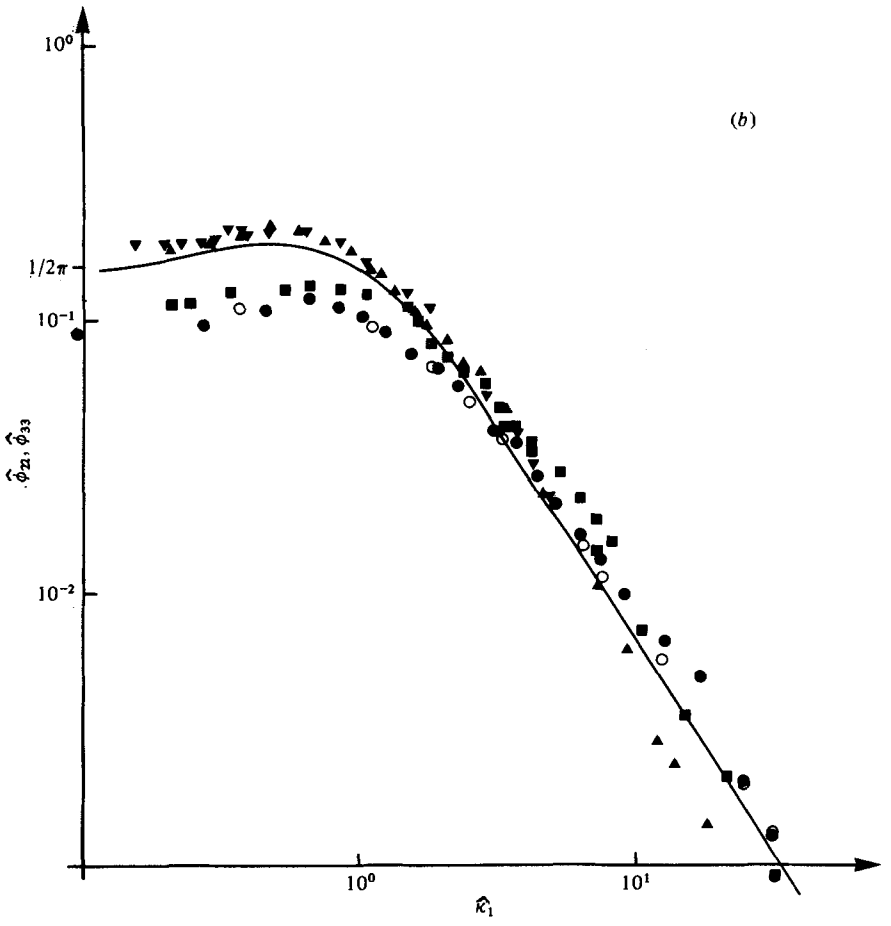

FIGURE 3. (*a*) The spectrum $\hat{\phi}_{11}(\hat{\kappa}_1)$ of longitudinal velocity fluctuations. (*b*) The spectra $\hat{\phi}_{22}(\hat{\kappa}_1)$ and $\hat{\phi}_{33}(\hat{\kappa}_1)$ of lateral (solid symbols) and axial (open symbols) velocity fluctuations u_2 and u_3. ——, von Kármán. $\hat{\kappa}_1 = 2\pi n L_x/\overline{U}_\infty$.

	●, ○	■	▲	▼
M (cm)	11·3	5·0	2·5	2·5
x_1/M	15·6	20	40	15
L_x (cm)	6·0	3·2	1·5	1·1

mesh size. This observation is supported by Jackson, Graham & Maull (1973), who found $L_{x2}/L_x \simeq 0{\cdot}38$ for a ratio of tunnel width to mesh size of approximately 7.

All spectra have been non-dimensionalized with the longitudinal integral scale. Combinations of the three grids and the three cylinders gave a range of a/L_x from 0·05 to 1·88. It should be noted that $\hat{\kappa}_1$ is effectively a *frequency*, non-dimensionalized with L_x and $\overline{U}_\infty$ throughout the flow. It is a wavenumber only in the upstream flow. In the vicinity of the cylinder, $\hat{\kappa}_1$ would correspond to a wavenumber if it were non-dimensionalized with the local mean velocity.

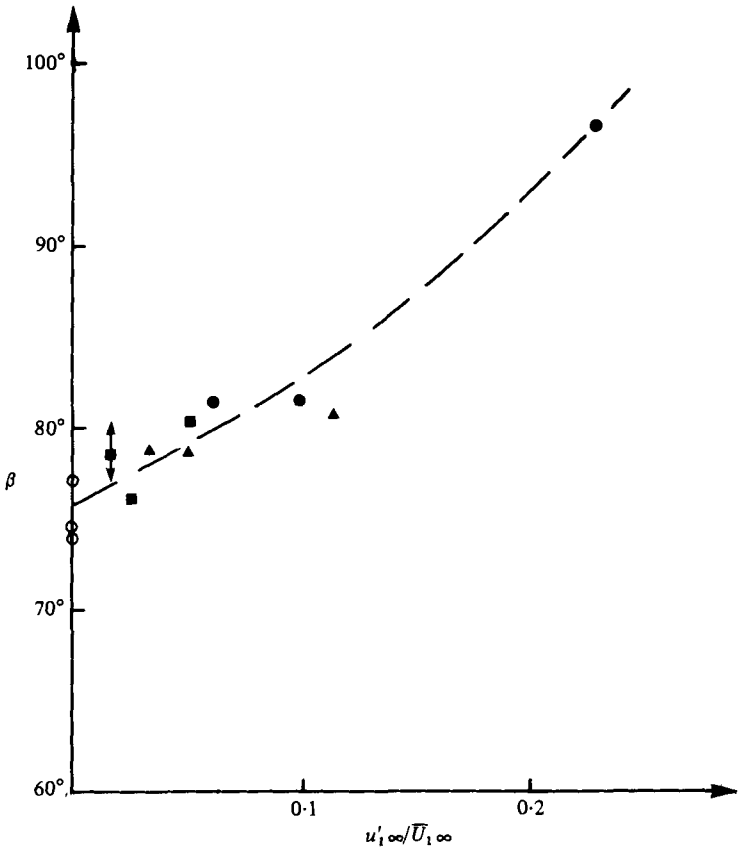

FIGURE 4. Angle β between line of stagnation and line of separation as a function of $u'_{1\infty}/\bar{U}_{\infty}$. ●, a/L_x = 0·4–0·6; ▲, a/L_x = 0·5–1·0; ■, a/L_x = 1·2–2·0.

4. Flow visualization and mean velocity measurements

Flow-visualization studies, using paraffin and titanium dioxide powder, were made to determine the influence of the incident turbulence on separation from the largest cylinder.

The results, presented in figure 4, indicate that separation was delayed as the intensity of turbulence was increased. At the extreme value of turbulence intensity (0·21), the cylinder was 0·381 m behind the 0·114 m grid. The flow must have been non-uniform with a probable ratio of maximum to minimum velocity of about 1·5 (Vickery 1966). Whether the dramatic delay of separation is a result of the high turbulence intensity or the non-uniform flow is uncertain. However, from the data of Bearman (1968) for the effect of free-stream turbulence on the critical Reynolds number, the effective critical Reynolds number would be far smaller than the cylinder Reynolds number of $2{\cdot}7 \times 10^4$ in the present experiments. Though the mean velocity is non-uniform the separation line was straight except close to the ends of the cylinder.

The three angles of separation for $u'_1/\bar{U}_{\infty} = 0{\cdot}001$ were 77·4, 74·5 and 74·1° with the cylinder at three different positions downstream from the end of the contraction (0·38, 1·02 and 1·78 m), which suggests that the position of separation is weakly

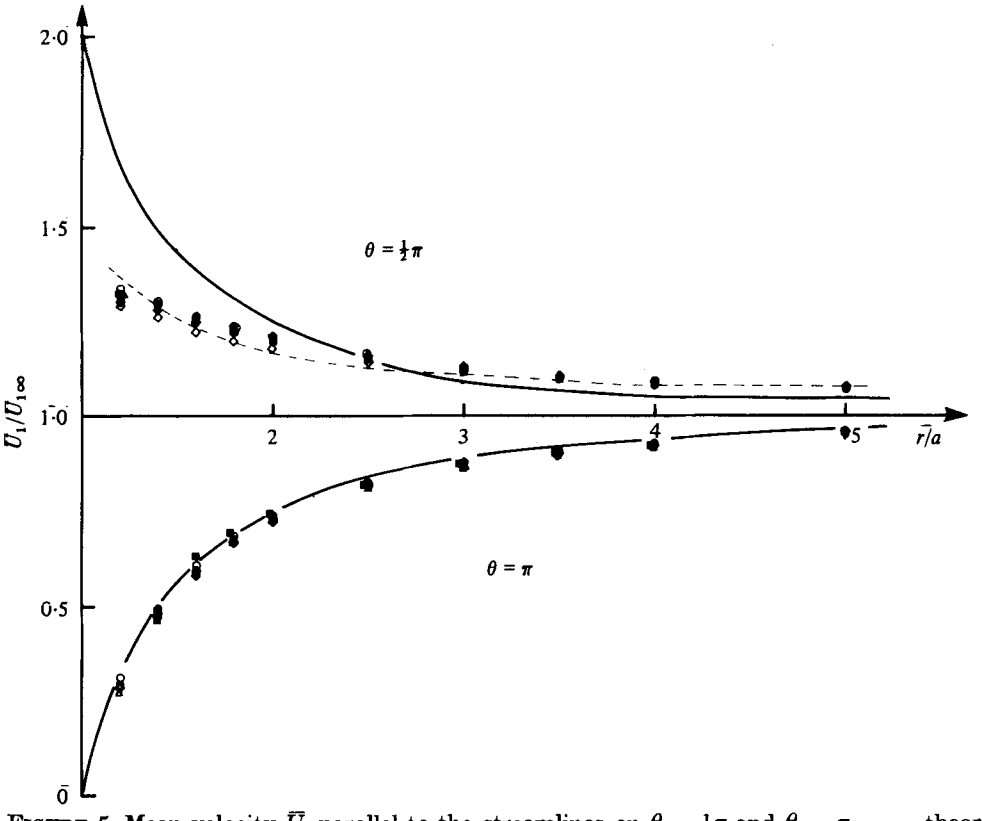

FIGURE 5. Mean velocity $\bar{U}_1$ parallel to the streamlines on $\theta = \frac{1}{2}\pi$ and $\theta = \pi$. ---, theoretical result based on the model of Parkinson & Jandali (1970); ——, potential flow with no separation.

	●, ○	□	△	■	◆	◇
M (cm)	11·3	5·0	2·5		No grid	
$u'_{1\infty}/\bar{U}_{1\infty}$	0·062	0·051	0·025		No grid	
L_x (cm)	6·0	3·2	1·5		No grid	
a (cm)	0·64, 2·06	2·06	2·06	0·32	0·64	2·06

influenced by the thickness of the wall boundary layers. The magnitudes of the mean velocity $\bar{U}_1$ along the stagnation line ($\theta = \pi$) and the cylinder centre-line ($\theta = \frac{1}{2}\pi$) are plotted in figure 5 for the full range of turbulence intensities covered in these experiments (0·001–6%).

The influence of the probe and probe support system on the flow around the cylinders was examined for the 0·0508 m grid at $x_1/M = 20$. The introduction of the probe along $\theta = \pi$ and $\theta = \frac{1}{2}\pi$ did not produce a change in the position of separation near the probe greater than the estimated experimental error of $\pm 1{\cdot}5°$, nor was there evidence of significant asymmetry in the line of separation except that for $\theta = \frac{1}{2}\pi$ and $r/a \leqslant 1{\cdot}4$ there was a delay in separation of a few degrees near the probe support. The separation line near the probe sensing element was less influenced. Separation from the $3{\cdot}18 \times 10^{-3}$ m radius cylinder at $x_1/M = 15{\cdot}6$ with the 0·114 m grid was delayed by $\simeq 5°$ for $\theta = \pi$ and $r/a \leqslant 2{\cdot}0$. On $\theta = \frac{1}{2}\pi$ separation was delayed by $\simeq 10°$ for $r/a = 1{\cdot}2$ and less than 5° for $r/a \geqslant 1{\cdot}4$.

The velocity variation along the stagnation line is similar to that predicted by

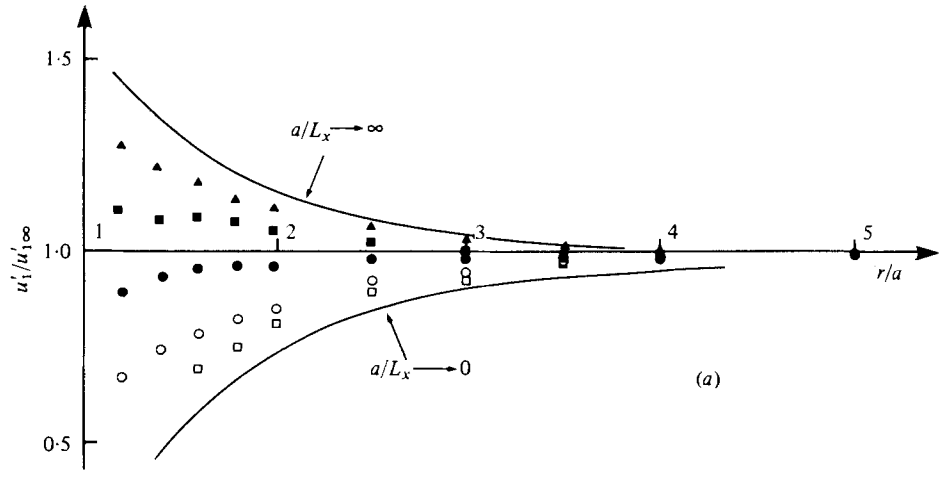

FIGURE 6(a). For legend see next page.

potential flow theory with no separation, particularly for the larger turbulence intensity. Along the line $\theta = \frac{1}{2}\pi$ the increase in mean velocity is substantially less than that predicted by a potential flow solution without separation. The results for the larger cylinder are, however, in general agreement with the wake source model of Parkinson & Jandali (1970); the mean velocity determined from their model for a negative base-pressure coefficient of 1·15 (typical for the present experiment) and a separation angle of $\beta = 80°$ is given in figure 5 for comparison. A (somewhat arbitrary) correction for blockage has been included by forcing the data to agree at $r/a = 5{\cdot}0$. The discrepancies in the measurements of $\overline{U}_1(r/a)$ along $\theta = \pi$ and along $\theta = \frac{1}{2}\pi$ are less than $\pm 5\%$ of $\overline{U}_\infty$. Their trends are consistent with the observation of turbulence delaying separation and their magnitude is consistent with the observed variation of 5 % of the separation angle. The direct effect of turbulent Reynolds stresses on $\overline{U}_1$ is negligible [H, equation (2.17)]. Another example of a highly strained turbulent flow where the turbulence does not affect the mean flow is the impinging jet (Miyazaki & Sparrow 1976). From the flow-visualization experiments and the mean velocity measurements, it may be concluded that the mean velocity field for $\theta \geqslant \frac{1}{2}\pi$ is not significantly altered by free-stream turbulence, or by the presence of the probe and probe support system.

5. Turbulence measurements

5.1. *Behaviour of the longitudinal velocity fluctuations u_1 on the stagnation line*

The ratio $u_1'/u_{1\infty}'$ of the local to the upstream r.m.s. value of the u_1 velocity fluctuations on the stagnation line is plotted in figure 6(*a*) and (*b*) as a function of r/a and a/L_x. The upstream value is taken at $r/a = 5{\cdot}0$. The results have been corrected to allow for the dissipation of turbulence in the absence of the cylinder,† as in the turbulence distortion experiments of Tucker & Reynolds (1968). This correction to the ratio of intensities was a maximum of 1, 1, 3, 5 and 4% for $a/L_x = 0{\cdot}05$, 0·11, 0·35, 0·64 and 1·42, respectively.

† Corrected values: $\overline{u_1^2}(r) = \overline{u_1^2}(r)|_{\text{meas}} + \overline{u_{1\infty}^2}|_{r/a=5} - \overline{u_{1\infty}^2}(r)$, where $\overline{u_{1\infty}^2}$ is the turbulence in the absence of the cylinder.

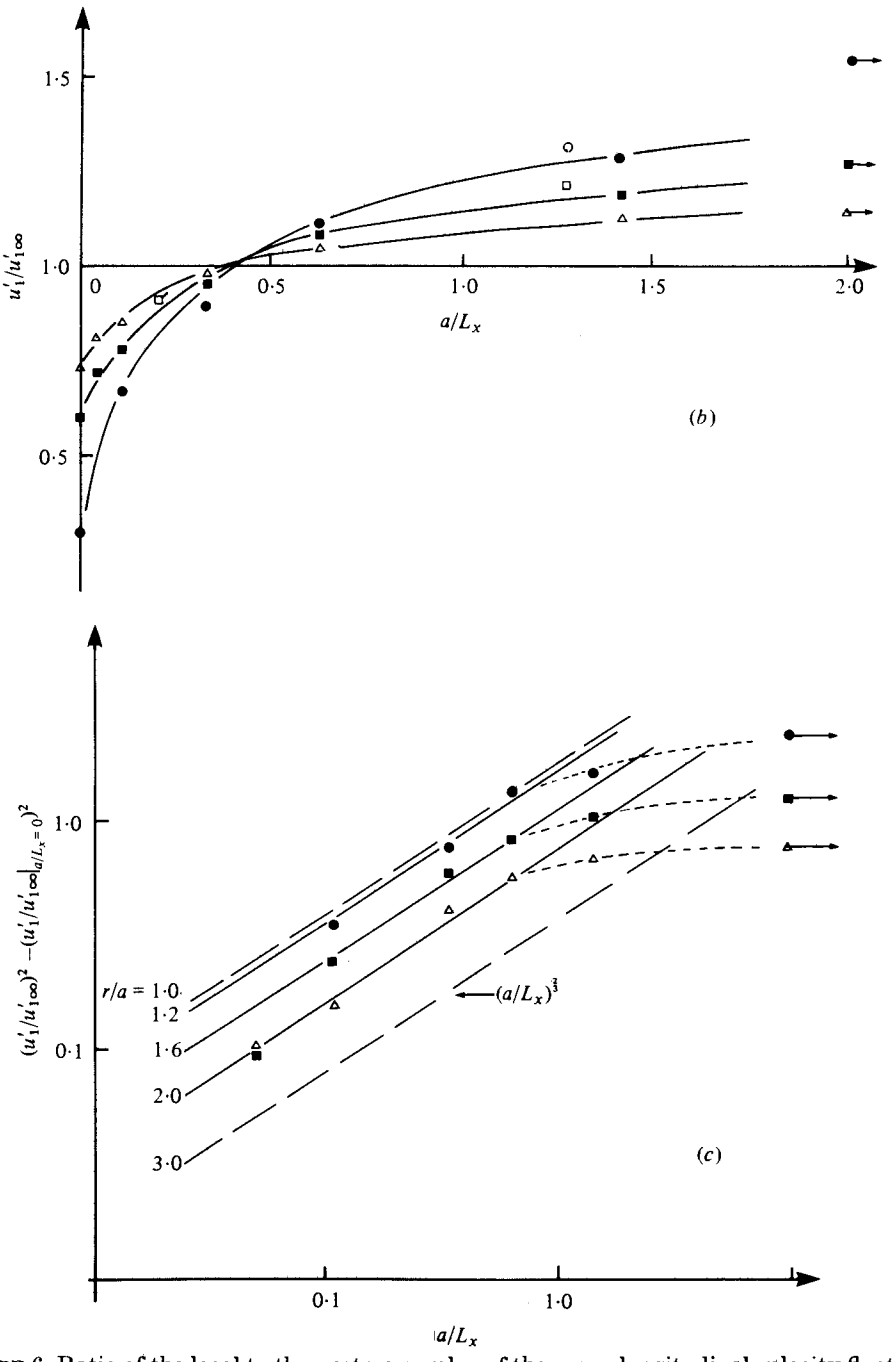

FIGURE 6. Ratio of the local to the upstream value of the r.m.s. longitudinal velocity fluctuations on the stagnation line ($\theta = \pi$) as a function of r/a and a/L_x. The effective values of r/a for a flat plate (Bearman 1972; □́) and a rectangular block (Todd & Walker: □, ○) are chosen such that $\overline{U}_1/\overline{U}_{1\infty}$ is the same as for a circular cylinder.

	□, □́	○	●	■	▲	△
(*a*) a/L_x	0·05	0·11	0·35	0·64	1·42	—
(*b*), (*c*) r/a	1·6	1·2	1·2	1·6	—	2·0

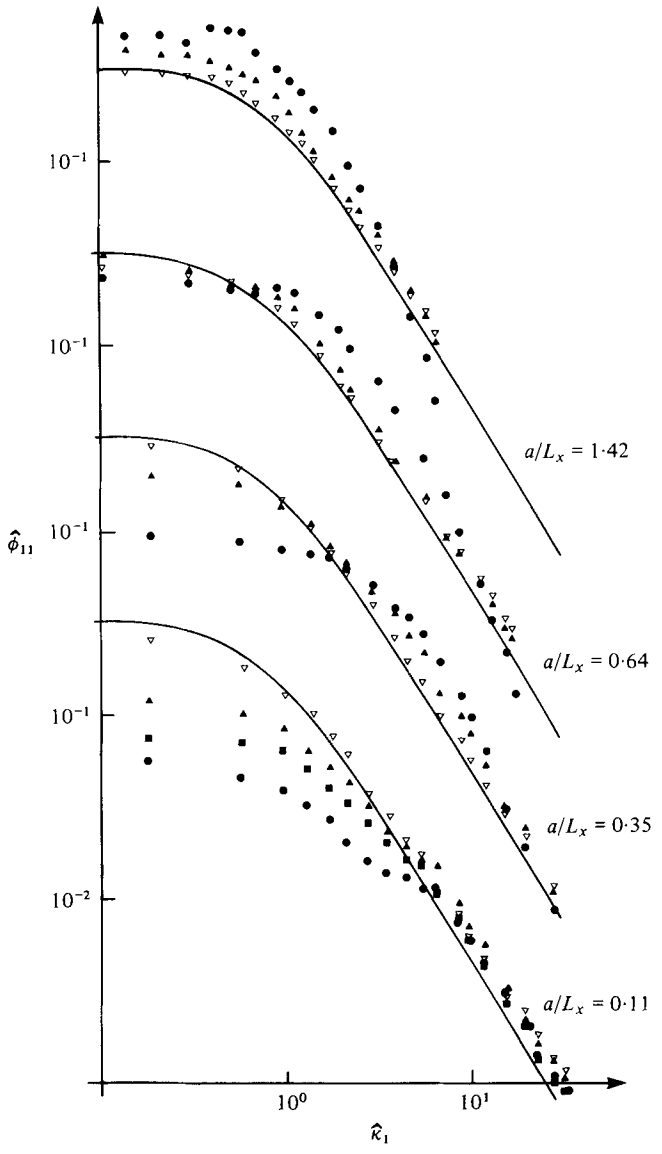

FIGURE 7. Variation of the spectrum of longitudinal velocity fluctuations on the stagnation line for $a/L_x = 0{\cdot}11, 0{\cdot}35, 0{\cdot}64, 1{\cdot}42$. The solid lines are equation (3.3).

	▽	▲	■	●
r/a	4·0	2·0	1·6	1·2

Figure 6 (a) includes the limiting curves for turbulence of very large scale (assuming the mean velocity to be given by potential flow with no separation), $a/L_x \to 0$, and for turbulence of very small scale, $a/L_x \to \infty$, as given in H. The ratio $u_1'/u_{1\infty}'$ increases monotonically as a/L_x increases between the two limiting curves as the numerical computation of H indicated should occur. The data in figure 6 (a) are cross-plotted in figure 6 (b) to show, specifically, the dependence of the turbulence distortion on the parameter a/L_x, the points for $a/L_x \to 0$ and $a/L_x \to \infty$ being taken from the limiting curves in figure 6 (a). For $a/L_x \simeq 0{\cdot}4$ the effects of blocking (in this

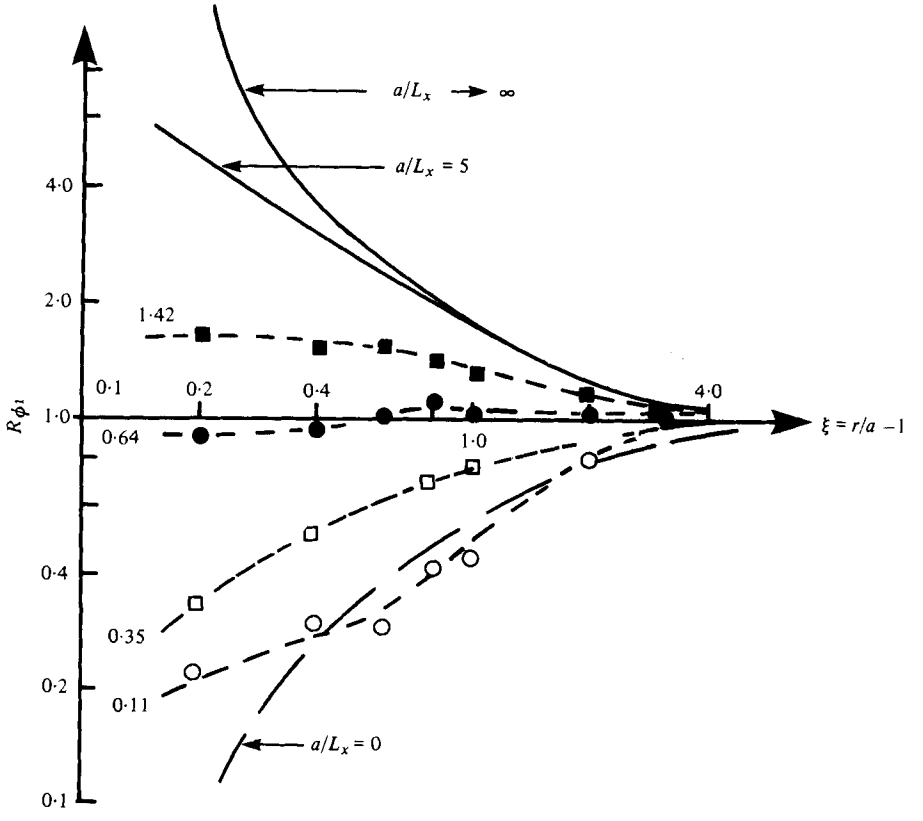

FIGURE 8. Variation of the low frequency components of the u_1 spectrum on the stagnation line compared with the theoretical forms when $a/L_x \to 0$ ($R_{\phi 1} = (\bar{U}_1/\bar{U}_{1\infty})^2$), $a/L_x \to \infty$ ($R_{\phi 1} = (\bar{U}_1/\bar{U}_{1\infty})^{-2}$) and $a/L_x = 5$ (see text).

case reducing) and vorticity distortion (in this case amplifying) apparently cancel for the range of r/a from 1·2 to 2·0. Unpublished experimental results of Petty (given by Hunt 1971) for turbulence around a circular cylinder agree with these results. Distortion of turbulence in a flow normal to a flat plate or a rectangular block can be compared with these results at the same value of $\bar{U}_1/\bar{U}_\infty$. Such results obtained by Bearman (1972) and Todd & Walker (given by Hunt 1976) are shown in figure 6(*b*).

From H it can be shown that as $a/L_x \to 0$, given $r/a = O(1)$, u_1' can be expanded as an asymptotic series:

$$\left(\frac{u_1'}{u_{1\infty}'}\right)^2 = \left(\frac{u_1'}{u_{1\infty}'}\right)^2\Bigg|_{a/L_x=0} + \left(\frac{a}{L_x}\right)^{\frac{2}{3}} f_1\left(\frac{r}{a}\right) + O\left[\left(\frac{a}{L_x}\right)^2\right], \tag{5.1}$$

where f_1 is $O(1)$ (see appendix). To test this prediction

$$\ln\{(u_1'/u_{1\infty}')^2 - (u_1'/u_{1\infty}')^2|_{a/L_x=0}\}$$

is plotted as a function of $\ln(a/L_x)$ in figure 6(*c*).

The spectra $\hat{\phi}_{11}(\hat{\kappa}_1)$ of the u_1 velocity fluctuations are presented in figure 7 for the same range of a/L_x and r/a. At low frequencies the ratio $R_{\phi 1}(\hat{\kappa}_1) = \hat{\phi}_{11}(\hat{\kappa}_1)/\hat{\phi}_{\infty 11}(\hat{\kappa}_1)$ of the spectrum to its upstream value is reduced at low values of a/L_x (by a factor of

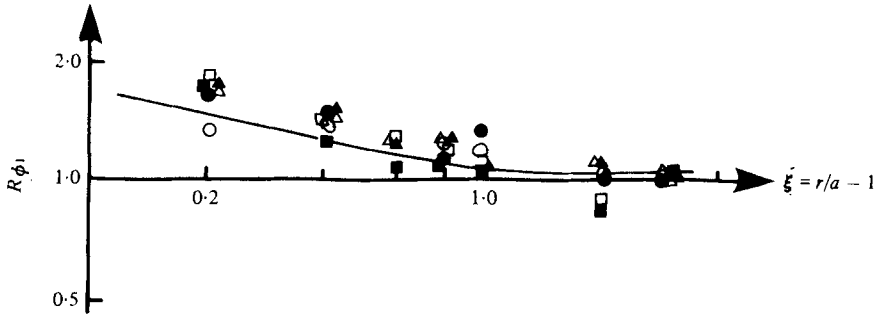

FIGURE 9. Variation of the high frequency components of the u_1 spectrum on the stagnation line compared with the theoretical form (which is proportional to $(\overline{U}_1/\overline{U}_{1\infty})^{-\frac{1}{3}}$ as $\xi \to 0$). $(a/L_x, \hat{\kappa}_1, \kappa_1)$: ○, (0·35, 2·80, 0·98); ●, (0·35, 5·04, 1·23); □, (0·64, 2·30, 1·47); ■, (0·64, 5·51, 3·53); △, (1·42, 0·68, 0·96); ▲, (1·42, 2·14, 3·14).

0·2 at $r/a = 1{\cdot}2$, $a/L_x = 0{\cdot}11$) and amplified as a/L_x increases (by 1·5 at $r/a = 1{\cdot}2$, $a/L_x = 1{\cdot}42$). At high frequencies the spectra are amplified for all values of a/L_x; the larger a/L_x the larger the range of $\hat{\kappa}_1$ over which amplification occurs.

To compare these results with the specific predictions of H, $R_{\phi 1}$ is plotted as a function of $\xi = r/a - 1$ for $\hat{\kappa}_1 \to 0$ and $\hat{\kappa}_1 \gg 1$ in figures 8 and 9. When $\hat{\kappa}_1 \to 0$ for large-scale turbulence ($a/L_x \ll 1$), the theory [H, equation (6.12)] suggests that

$$R_{\phi 1} = (\overline{U}_1/\overline{U}_{1\infty})^2, \tag{5.2}$$

which is the curve plotted in figure 8. But when $\hat{\kappa}_1 \to 0$ for small-scale turbulence ($a/L_x \gg 1$), the spectrum is amplified by an amount that depends on the distance from the cylinder ξa and the ratio $\xi a/L_x$ of this distance to the integral scale. When

$$(a/L_x)\,\xi \gg 1, \quad R_{\phi 1} = (\overline{U}_1/\overline{U}_{1\infty})^{-2}. \tag{5.3}$$

When $(a/L_x)\,\xi$ is $O(1)$ and $\xi \ll 1$ the effect of the blocking of the cylinder surface (or the image vorticity within the cylinder) is accounted for by a local function $G(a\xi/L_x)$:

$$R_{\phi 1} = (\overline{U}_1/\overline{U}_{1\infty})^{-2}\, G(a\xi/L_x),$$

where $G \to 1$ when $a\xi/L_x \gg 1$ and $G \sim 0{\cdot}618\xi^{\frac{5}{3}}$ when $a\xi/L_x \ll 1$. The function

$$G(a\xi/L_x)$$

can be obtained from equations (6.36) and (6.47) in H (see also figure 13 in H) for the case where $a/L_x \gg 1$ (in which case G varies only where $\xi \ll 1$). In figure 8, $R_{\phi 1}(\xi)$ is plotted for $a/L_x \to \infty$ and for typical large, but finite, values of a/L_x. Our largest value of a/L_x is not large enough for $R_{\phi 1}$ to be estimated by the asymptotic theory. Recently Gutmark *et al.* (1978) successfully compared the above theory with measurements of $R_{\phi 1}(\kappa_1 = 0)$ in a two-dimensional jet impinging on a plate.

At frequencies sufficiently high that $\hat{\kappa}_1 a/L_x \gg 1$, the asymptotic theory suggests that $R_{\phi 1}$ is a function only of r/a for all a/L_x. This curve is compared with the experimental points in figure 9. When $r/a \to 1$ the theoretical asymptotic limit is

$$R_{\phi 1} = 0{\cdot}86\overline{U}_1^{-\frac{1}{3}}$$

so the amplification is much lower than when $\hat{\kappa}_1 \to 0$.

5.2. *The effects of wake-induced velocity fluctuations*

The subject of the present study is the variation of $u_i^{(T)}$ as a result of the flow around a circular cylinder. With the neglect of nonlinear turbulent interactions (including any nonlinear interaction between the rotational $u_i^{(T)}$ and the irrotational $u_i^{(w)}$), the variation of $u_i^{(T)}$ is completely determined by the mean velocity field and the proximity of rigid boundaries. It has been shown that the mean velocity field is not significantly altered by free-stream turbulence, nor by the presence of the probe and probe support system.

In contrast, the wake-induced velocity fluctuations (in particular the vortex-shedding 'spike') were strongly influenced by free-stream turbulence (as expected from the results of Gerrard 1965), the thickness of the tunnel wall boundary layers, the Reynolds number, the position of the probe and probe support systems, the tunnel blockage and probably the aspect ratios of the cylinders. These effects are of interest in the present work only in their contamination of $u_i^{(T)}$.

Since $u_i^{(w)\prime}/\overline{U}_\infty$ is small (typically less than 0·05 for $\theta > \frac{1}{2}\pi$ and $r/a > 1{\cdot}1$), it is reasonable to assume that $u_i^{(T)}$ and $u_i^{(w)}$ are statistically independent, in which case

$$\overline{u_i^2} = \overline{u_i^{(T)2}} + \overline{u_i^{(w)2}}. \tag{5.4a}$$

In the limit of very *weak* ($\ll 1\%$) upstream turbulence $\overline{u_i^{(w)2}}$ is unaffected by the upstream turbulence, so that as $u'_{1\infty}/\overline{U}_\infty \to 0$

$$\overline{u_i^2} = \overline{u_i^{(T)2}} + \overline{u_i^{(w,0)2}}, \tag{5.4b}$$

where $u_i^{(w,0)}$ is the velocity induced by the wake turbulence in the absence of upstream turbulence. Equation (5.4*b*) is sometimes used as an approximation for finding $\overline{u_i^{(T)2}}$ even when it is not strictly valid. The assumption (5.4*a*) was used in the theory of H. It implies, for example, that $\overline{u_i^{(w)} u_i^{(T)}} = 0$, but does not exclude $u_i^{(w)}$ and the spectrum $\phi_{ii}^{(w)}$ of $u_i^{(w)}$, being functions of $u'_{1\infty}/\overline{U}_\infty$ and a/L_x, in which case (5.4*b*) cannot be used to separate $\overline{u_i^{(T)2}}$ and $\overline{u_i^{(w)2}}$. One possibility that was investigated was the use of both the independence of the spectra $\phi_{ii}^{(T)}$ and $\phi_{ii}^{(w)}$, which implies that

$$\phi_{ii} = \phi_{ii}^{(T)} + \phi_{ii}^{(w)}, \tag{5.5}$$

and the hypothesis that the major component of $\phi_{ii}^{(w)}$ is due to vortex shedding. The wake spectrum $\phi_{ii}^{(w)}$ is certainly affected by the upstream turbulence both in the amplitude and in the width of the 'spike' due to vortex shedding. Inspection of the ϕ_{ii} spectra suggests that one could obtain an estimate of $\phi_{ii}^{(T)}$ by interpolating between values of ϕ_{ii} either side of the vortex-shedding 'spike', and hence obtain $\overline{u_i^{(T)2}}$ by integration. Unfortunately, the spectral resolution was not always sufficient for this procedure to be reliable.

On the stagnation line, in the absence of free-stream turbulence, both u_1 and the axial velocity fluctuations u_3 are small ($u_{1,3}^{(w,0)\prime}/\overline{U}_{1\infty} \leqslant 0{\cdot}003$) and negligible in comparison with the grid-generated turbulence used in the present experiments. It is expected that $u_3^{(w)\prime}$ would be small everywhere forward of separation, its magnitude falling off as the inverse fourth power of the distance from the wake (see §6.2). On $\theta = \pi$, $u_2^{(w)\prime}$ is negligible for all a/L_x other than 1·42 (the free-stream turbulence was considerably less for this value than for the others). For the u_1 and u_2 components on $\theta = \frac{1}{2}\pi$ there

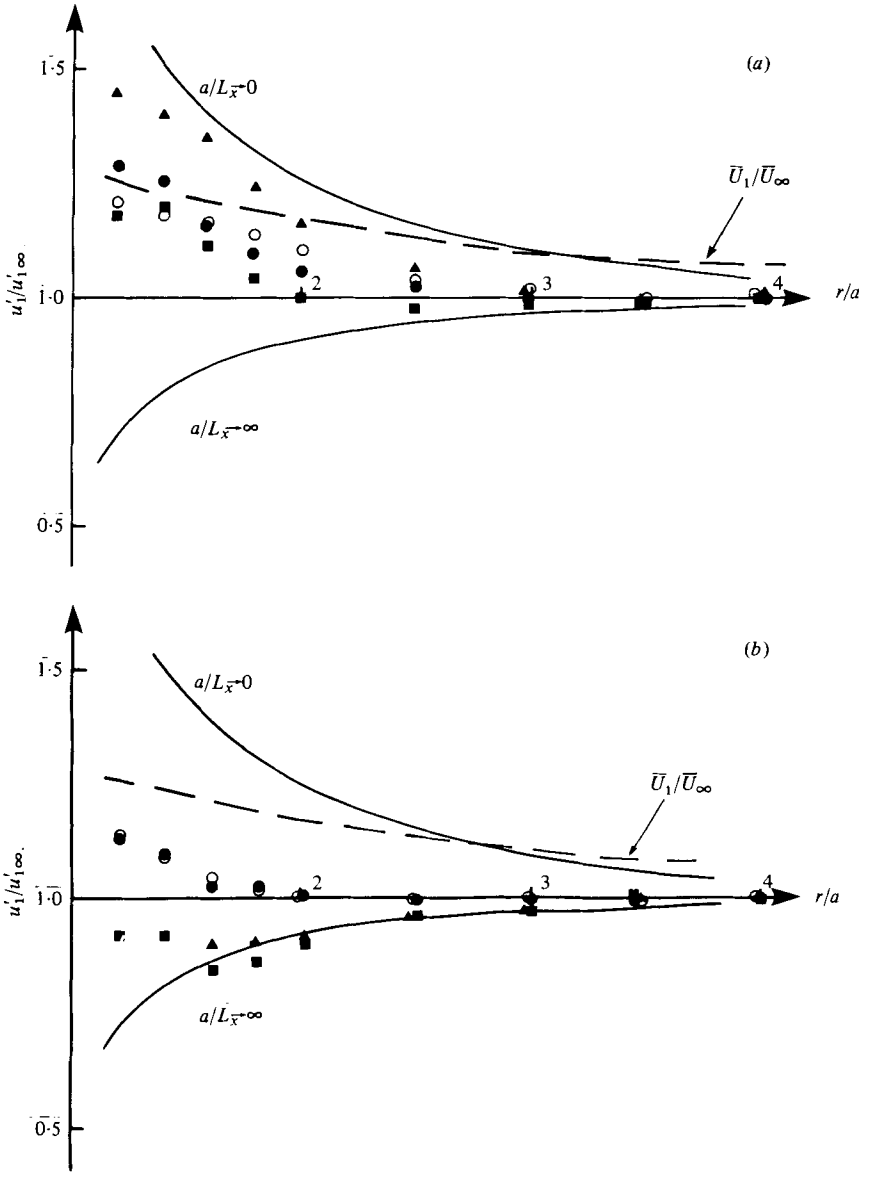

FIGURE 10. Ratio of the local to the upstream value of the r.m.s. streamwise velocity fluctuations on the line $\theta = \frac{1}{2}\pi$ (*a*) as a function of r/a and a/L_x and (*b*) from the integrated spectra ignoring the vortex-shedding peak.

a/L_x	○ 0·11	● 0·35	■ 0·64	▲ 1·88

was serious contamination of $u_i^{(T)\prime}$ by wake-induced fluctuations. The value of $u_1^{(T)\prime}$ on $\theta = \frac{1}{2}\pi$ has been estimated by integrating the spectra ignoring the vortex-shedding spike. This procedure was not adequate for estimating $u_2^{(T)\prime}$ on $\theta = \frac{1}{2}\pi$ and the measurements of u_2' (figure 15) are presented for completeness only (though the data for $a/L_x = 0{\cdot}11$ and $a/L_x = 1{\cdot}88$ with a splitter plate are little influenced by $u_2^{(w)\prime}$). Nevertheless, even under the worst conditions, the spectral results can be used to isolate

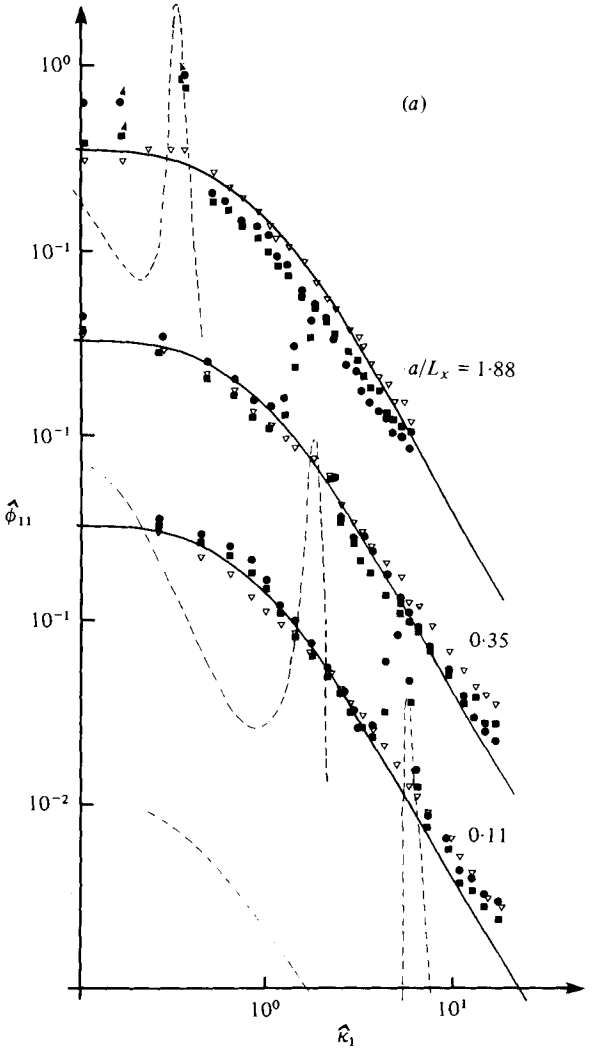

FIGURE 11 (*a*). For legend see next page.

frequency bands in which ϕ_{ii} was principally $\phi_{ii}^{(T)}$; for example, at all frequencies above the vortex-shedding frequency $\phi_{ii}^{(w)} \ll \phi_{ii}^{(T)}$. In addition, provided that

$$u_i^{(w)\prime}/u_i^{(T)\prime} \lesssim 1$$

there is often a band of frequencies below the vortex-shedding frequency for which $\phi_{ii}^{(w)} \ll \phi_{ii}^{(T)}$. In this frequency band ϕ_{ii} may be treated as $\phi_{ii}^{(T)}$. Another possible method of distinguishing between $u_i^{(T)}$ and $u_i^{(w)}$ is to attach a splitter plate to the cylinder (on $\theta = 0$), and thus eliminate the vortex shedding, which gives the largest contribution to $u_i^{(w)}$. The experiments, however, indicated that, although the vortex-shedding 'spike' was significantly attenuated by the inclusion of a splitter plate, the low frequency content of the vortex-shedding signal was enhanced, and the net effect of the splitter plate was a reduction in intensity by a factor of less than 2.

There is, however, a serious objection to the use of a splitter plate in the present

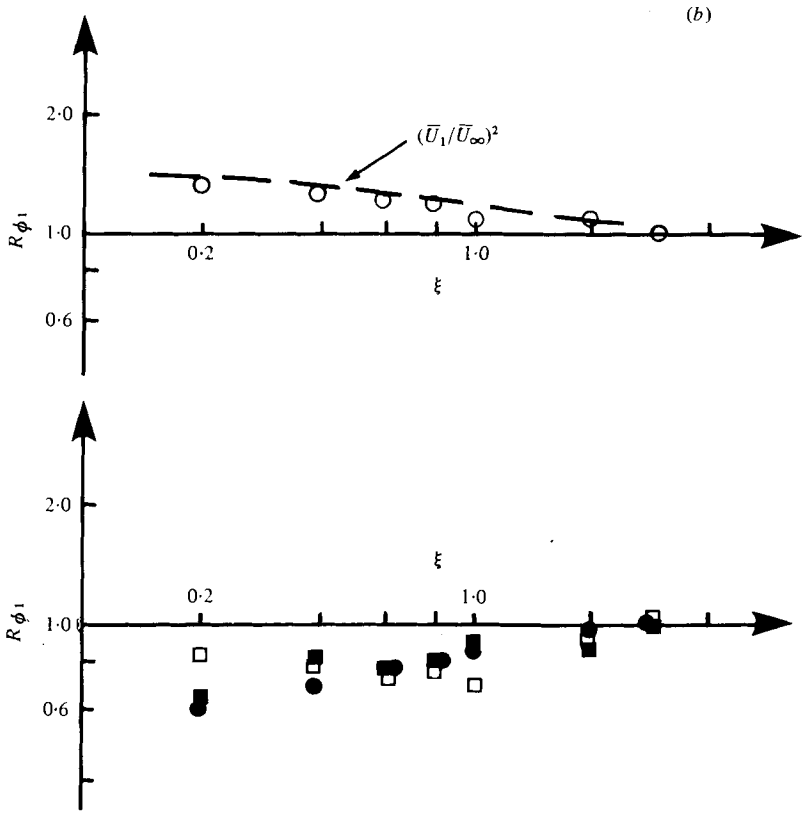

FIGURE 11. (*a*) Variation of the spectrum of the longitudinal velocity fluctuations on $\theta = \frac{1}{2}\pi$ for $a/L_x = 1{\cdot}88$, $0{\cdot}35$ and $0{\cdot}11$. ---, spectra taken at $r/a = 1{\cdot}6$ when there is no upstream turbulence. ▽, $r/a = 4{\cdot}0$; ■, $r/a = 1{\cdot}6$; ●, $r/a = 1{\cdot}2$. (*b*) Variation of the high and low frequency components of the u_1 spectrum on $\theta = \frac{1}{2}\pi$. (a/L_x, $\hat{\kappa}_1$, κ_1): ○, ($0{\cdot}11$, $0{\cdot}14$, $0{\cdot}015$); □, ($0{\cdot}35$, $9{\cdot}60$, $3{\cdot}36$); ●, ($0{\cdot}64$, $10{\cdot}32$, $6{\cdot}60$); ■, ($1{\cdot}88$, $4{\cdot}89$, $9{\cdot}19$); ---, theoretical form for $a/L_x \to 0$, $\kappa_1 \to 0$.

experiments. In the limit $a/L_x \to 0$ the cylinder is located in a velocity field whose direction and magnitude are varying slowly with time. The distortion of this turbulent velocity field, and in particular the lateral velocity fluctuations, must be strongly influenced by a splitter plate behind the cylinder. Results obtained when a splitter plate was fixed to the cylinder were markedly different to those obtained without a splitter plate, except for the smallest scales of turbulence; see §5.4.

5.3. *Behaviour of streamwise velocity fluctuations on* $\theta = \frac{1}{2}\pi$

Along the centre-line of the cylinder ($\theta = \frac{1}{2}\pi$), the mean flow direction varies between about 10 and 0° to the x axis as r/a increases. The measurements of r.m.s. turbulent velocity fluctuations u_1' parallel to the mean flow are plotted in figure 10(*a*) as the ratio to $u_{1\infty}'$ and as a function of r/a. A significant part of the velocity fluctuations is contributed by the wake component $u_1^{(w)}$.

The spectra $\hat{\phi}_{11}(\hat{\kappa}_1)$ of u_1 on $\theta = \frac{1}{2}\pi$ are presented in figure 11(*a*). For the largest scale of turbulence, $a/L_x = 0{\cdot}11$, the spectrum is systematically amplified at low wavenumbers. This amplification is compared in figure 11(*b*) with that predicted by

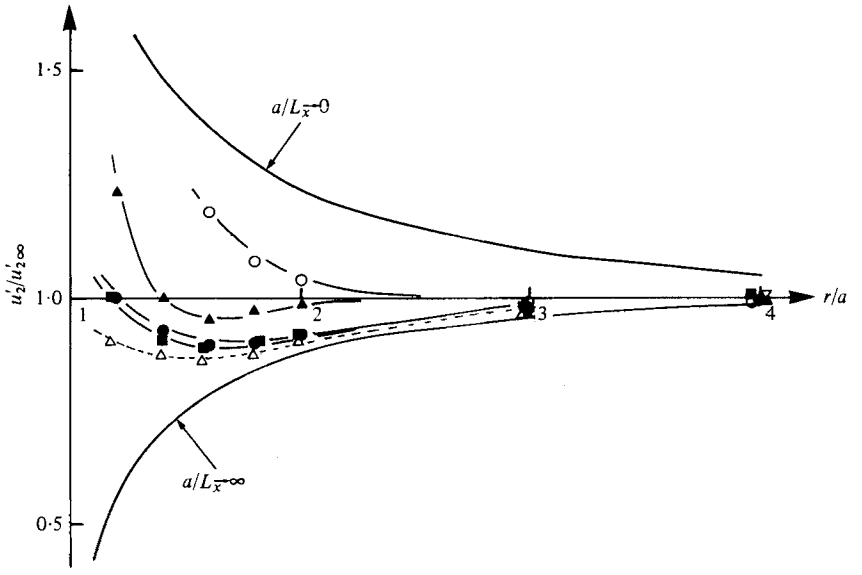

FIGURE 12. Ratio of the local to the upstream value of the r.m.s. lateral velocity fluctuations u_2 on the stagnation line $\theta = \pi$ as a function of r/a and a/L_x. Results with a splitter plate attached, for $a/L_x = 1{\cdot}42$, are included.

	○	●	■	▲	△
a/L_x	0·11	0·35	0·64	1·42	1·42 + splitter plate

a quasi-steady analysis, i.e. spectral energy density proportional to $\overline{U}_1^2$. For $\hat{\kappa}_1 > 1$ there is little amplification. When $\hat{\kappa}_1 > 10$ there is small attenuation of spectral energy as the cylinder is approached. For $a/L_x = 0{\cdot}35$ and $0{\cdot}64$ there is also amplification at low wavenumbers. However, at higher wavenumbers there is significant attenuation of the spectra as the cylinder surface is approached. For the smaller scales ($a/L_x = 1{\cdot}88$) there is attenuation of the spectra at all wavenumbers, other than those which might be influenced by vortex shedding, i.e. for $\hat{\kappa}_1 > 0{\cdot}8$. Careful inspection of all the spectra for $a/L_x = 0{\cdot}35$, $0{\cdot}64$ and $1{\cdot}88$ shows that for a range of wavenumbers the spectra are first attenuated as the cylinder is approached but are then amplified close to the cylinder (or, more correctly, close to the separation streamline). This range of wavenumbers scales on the cylinder radius.

It is interesting that for all values of a/L_x and r/a the vortex-shedding peak is altered by the incident turbulence in that it is at a slightly lower frequency, is broader and is of greater amplitude. It was found that the strength of vortex shedding (area of shedding peak) was strongly influenced by the interaction of the flow around the cylinder with the growing boundary layer on the tunnel walls. With very low intensity incident turbulence (no grid), it was observed that the strength of the vortex shedding was increased by increasing the ratio of the cylinder diameter to tunnel boundary-layer thickness. While this was not unexpected, somewhat more surprising was the observation that the introduction of free-stream turbulence apparently disrupted the interaction at the ends of the cylinder and resulted in an increase in the strength of vortex shedding. Thus some of the increase in the strength of vortex shedding in figure 11(*a*) is a result of the modified end flow. However, even with the use of end plates to isolate the tunnel boundary layers a significant increase in the strength of

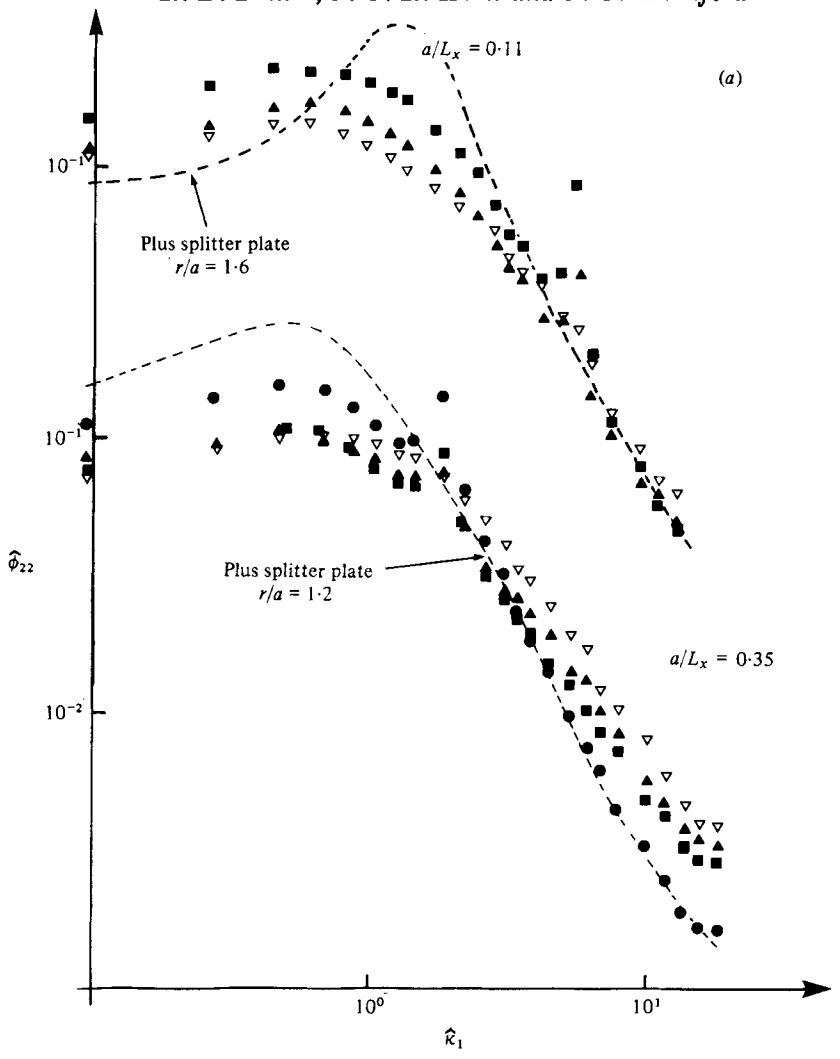

FIGURE 13(a). For legend see facing page.

vortex shedding was observed, for all r/a and all a/L_x, with the introduction of free-stream turbulence. These observations are in qualitative agreement with those of Gerrard (1965).

The spectra in figure 11(a) have been integrated (with the vortex-shedding peak removed) to give estimates of $u_1^{(T)'}$ and these are presented in figure 10(b).

5.4. *Behaviour of the lateral velocity fluctuations on* $\theta = \pi$

The variation of the r.m.s. value u_2' of the lateral component of velocity fluctuations on the stagnation line, $\theta = \pi$, is shown in figure 12. A dissipation correction was applied (see §5.1). The results lie within the two asymptotic limits, those for $a/L_x = 0{\cdot}11$ showing the expected amplification and those for $a/L_x = 0{\cdot}35$ and $0{\cdot}64$ being attenuated. The result for $a/L_x = 1{\cdot}42$ is dominated by vortex shedding.

The spectra in figure 13 show that at low frequencies and large scales ($a/L_x < 0{\cdot}4$) the ratio $R_{\phi 2} = \hat{\phi}_{22}(\hat{\kappa}_1)/\hat{\phi}_{\infty 22}(\hat{\kappa}_1)$ is amplified near the cylinder, but that for smaller

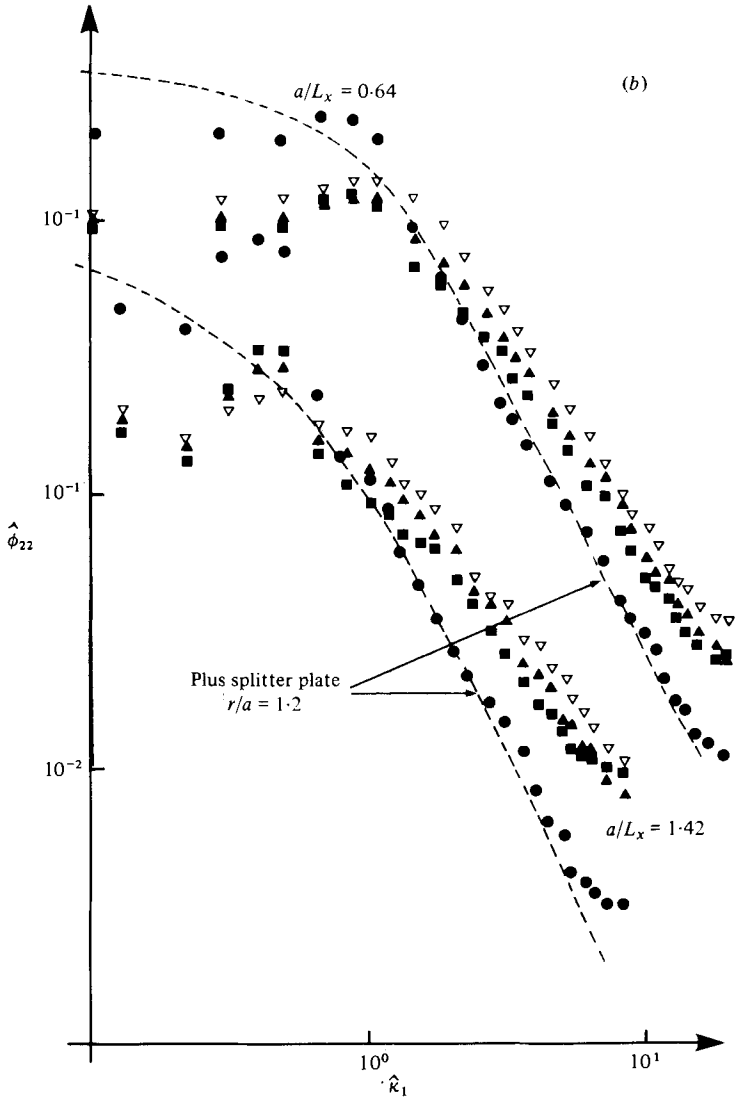

FIGURE 13. Variation of the spectrum of the lateral velocity fluctuations u_2 on the stagnation line $\theta = \pi$ for (*a*) $a/L_x = 0{\cdot}11$ and $0{\cdot}35$ and (*b*) $a/L_x = 0{\cdot}64$ and $1{\cdot}42$. The influence of a splitter plate is shown by the dashed line. ▽, $r/a = 4{\cdot}0$; ▲, $r/a = 2{\cdot}0$; ■, $r/a = 1{\cdot}6$; ●, $r/a = 1{\cdot}2$.

scales ($a/L_x > 0{\cdot}6$) $R_{\phi 2}$ first slightly *decreases* and then increases close to the surface. To demonstrate the first of these effects $R_{\phi 2}$ is plotted as a function of $\xi = r/a - 1$ for $\kappa_1 \ll 1$ and $a/L_x \ll 1$ in figure 14, and compared with the theoretical prediction (H, or equation (6.12) or figure 9).

Figure 13 also shows that at high frequencies, for all values of a/L_x, $R_{\phi 2}$ decreases near the cylinder. $R_{\phi 2}$ is plotted in figure 14 as a function of ξ for $\hat{\kappa}_1 a/L_x \simeq 3{\cdot}5$, and compared with the theoretical prediction computed from H, equations (6.30) and (6.31), which is valid only when $(\hat{\kappa}_1 a/L_x)\xi \gg 1$ and $\hat{\kappa}_1 a/L_x \gg 1$.

The behaviour of $\hat{\phi}_{22}(\hat{\kappa}_1)$ on the stagnation line also illustrates the effect of a splitter plate. This effectively reduces or removes the vortex-shedding peak and also produces

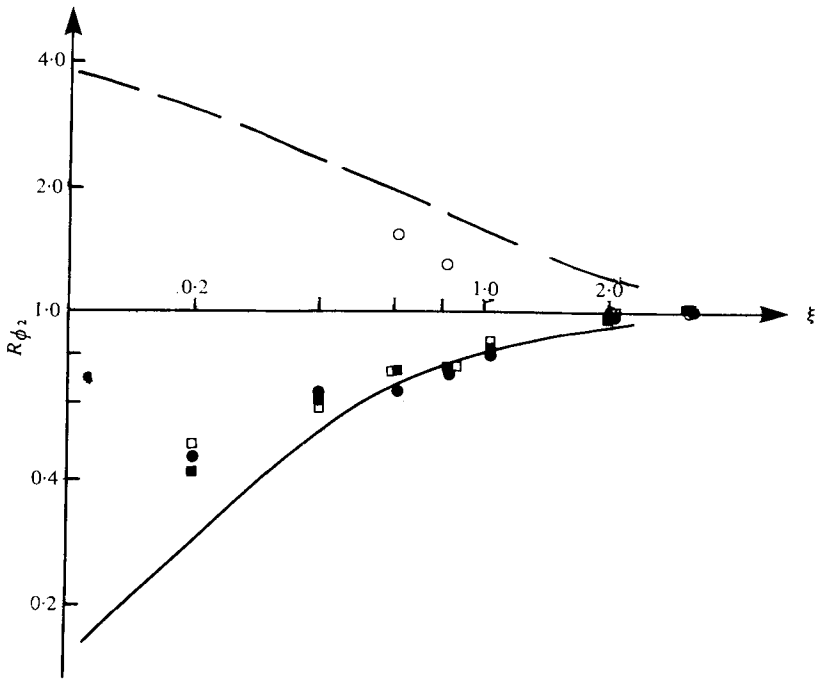

FIGURE 14. Variation of the high and low frequency components of the spectrum of the lateral velocity fluctuations u_2 on the stagnation line $\theta = \pi$ compared with theory when $\kappa_1 \gg 1$ and $\kappa_1(r/a-1) \gg 1$ (solid curve) and when $a/L_x \ll 1$ and $\kappa_1 \ll 1$ (dashed curve). $(a/L_x, \kappa_1, \kappa_1)$: ○, (0·11, 0·3, 0·03); ●, (0·35, 9·60, 3·4); □, (0·64, 5·65, 3·6); ■, (1·42, 2·47, 3·5).

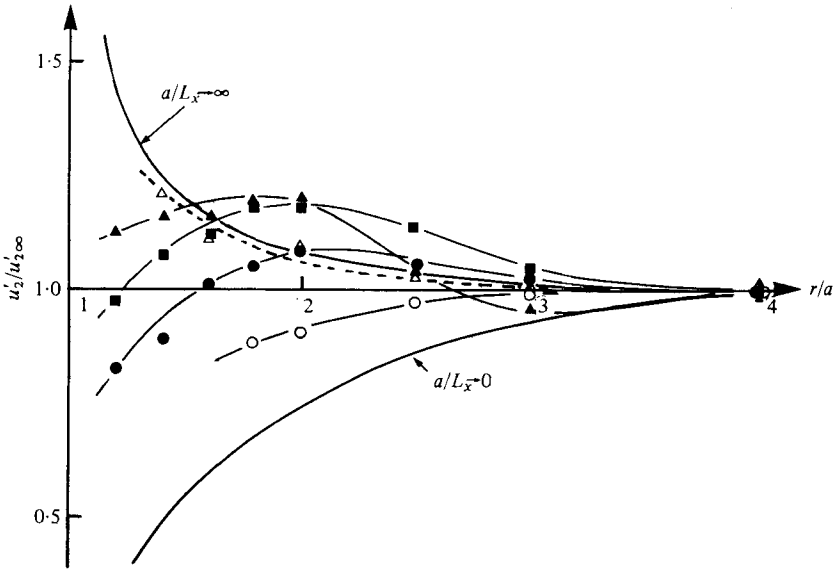

FIGURE 15. Ratio of the local to the upstream values of the r.m.s. lateral velocity fluctuations on $\theta = \frac{1}{2}\pi$ as a function of r/a and a/L_x. Results with a splitter plate are included for $a/L_x = 1{\cdot}88$.

	○	●	■	▲	△
a/L_x	0·11	0·35	0·64	1·88	1·88 + splitter plate

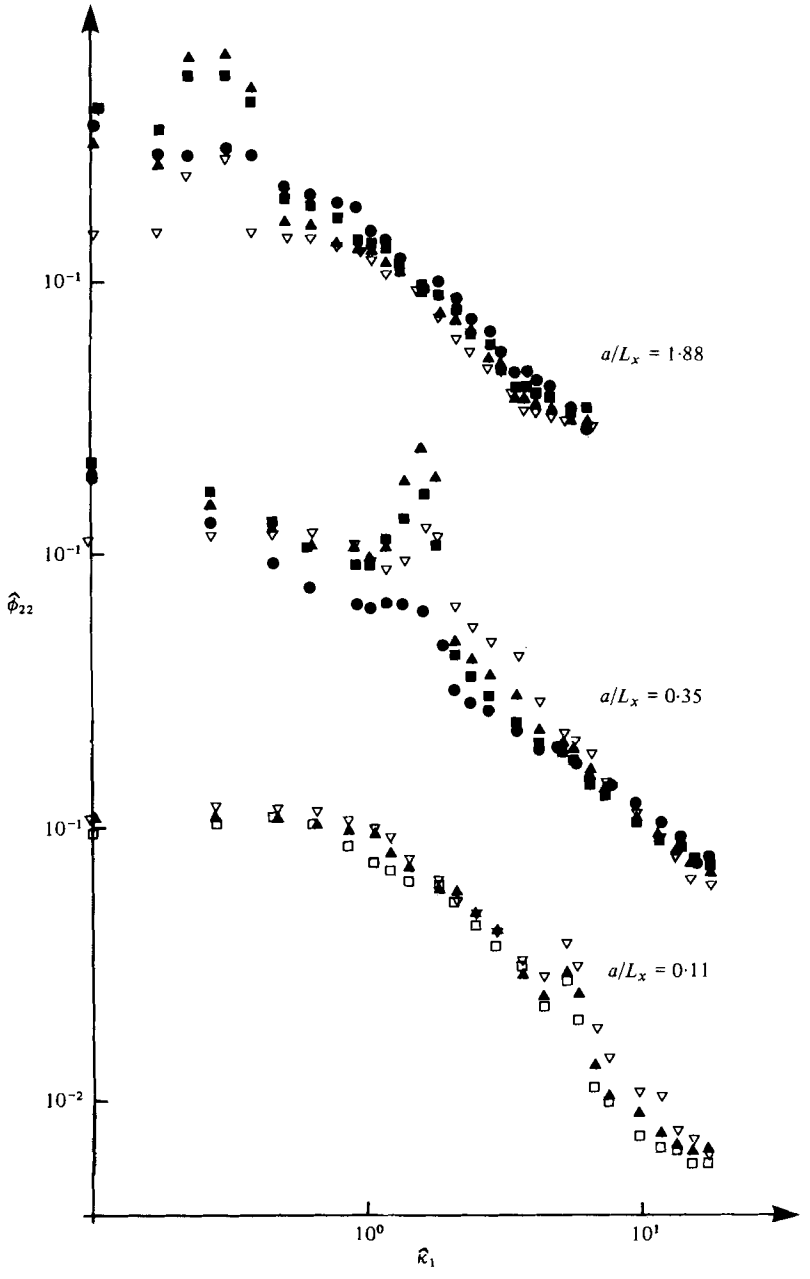

FIGURE 16. Variation of the spectrum of the lateral velocity fluctuations on $\theta = \frac{1}{2}\pi$ for $a/L_x = 1{\cdot}88$, $0{\cdot}35$ and $0{\cdot}11$.

	▽	▲	□	■	●
r/a	4·0	2·0	1·8	1·6	1·2

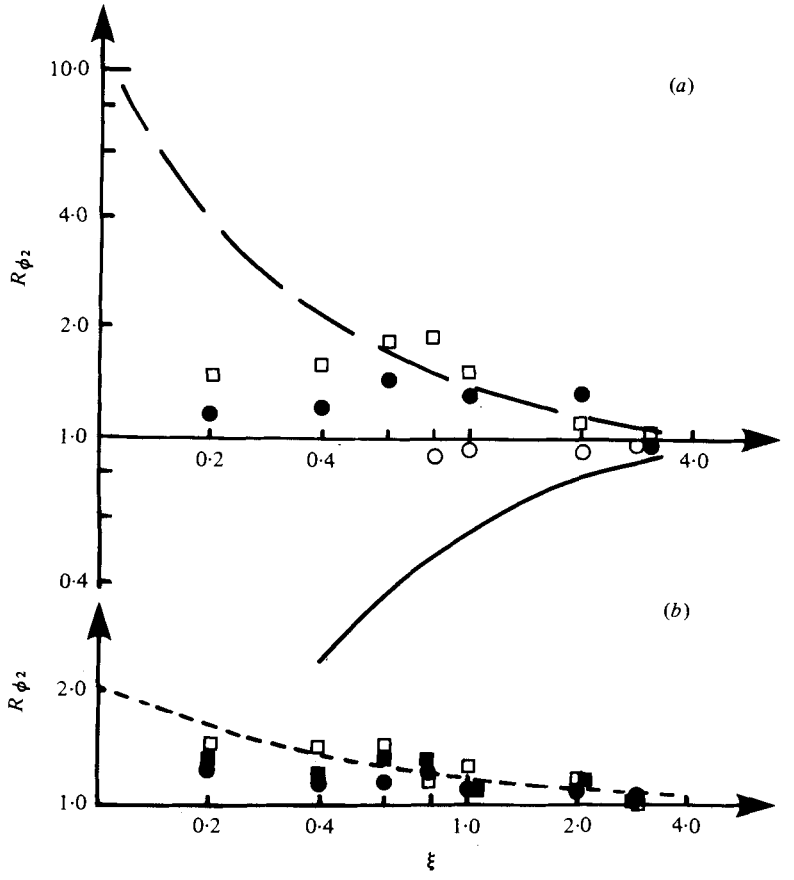

FIGURE 17. Variation of the high and low frequency components of the lateral velocity fluctuations compared with theory. (*a*) When $a/L_x \to 0$ (solid curve) and $a/L_x \gg 1$, $\kappa_1 = 0$ (dashed curve). (a/L_x, $\mathcal{K}_1$, κ_1): ○, (0·11, 0·3, 0·03); ●, (0·35, 0·3, 0·11); □, (0·64, 0·3, 0·19). (*b*) When $\kappa_1 \gg 1$, $\xi\kappa_1 \gg 1$. (a/L_x, $\mathcal{K}_1$, κ_1): ●, (0·35, 17·1, 6·0); □, (0·64, 14·3, 9·1); ■, (1·88, 5·6, 10·5).

a significant change in the spectrum at frequencies less than the vortex-shedding frequency. The change in the spectrum at low frequencies is unlikely to be due solely to a change in $\hat{\phi}_{22}^{(w)}$ as $\phi_{22}^{(w,0)}$ is less than $\frac{1}{30}\phi_{22}$ with free-stream turbulence (for $a/L_x = 0{\cdot}35$).

5.5. *Behaviour of the lateral velocity fluctuations u_2 on $\theta = \frac{1}{2}\pi$*

Measurements on the centre-line of the cylinder ($\theta = \frac{1}{2}\pi$) of the ratio $u_2'/u_{2\infty}'$ of the lateral velocity fluctuations to their upstream value are plotted as a function of r/a and a/L_x in figure 15. The trend of $u_2'/u_{2\infty}'$ with a/L_x roughly follows the theory, but the values of $u_2'/u_{2\infty}'$ are not contained within the asymptotic limits.

The spectra in figure 16 confirm that the cause of the anomalous amplification is the vortex shedding. The amplification of the spectra $R_{\phi 2}$ is plotted in figure 17, with the theoretical predictions. For the largest scale ($a/L_x = 0{\cdot}11$), at low frequency the reduction in $R_{\phi 2}$ is 0·85 at $r/a = 1{\cdot}8$ whereas for the small scale ($a/L_x = 0{\cdot}64$) the amplification at $r/a = 1{\cdot}8$ is about 2·0. At high frequencies, a smaller amplification is observed ($R_{\phi 2} = 1{\cdot}5$ at $r/a = 1{\cdot}2$ and $a/L_x = 1{\cdot}88$).

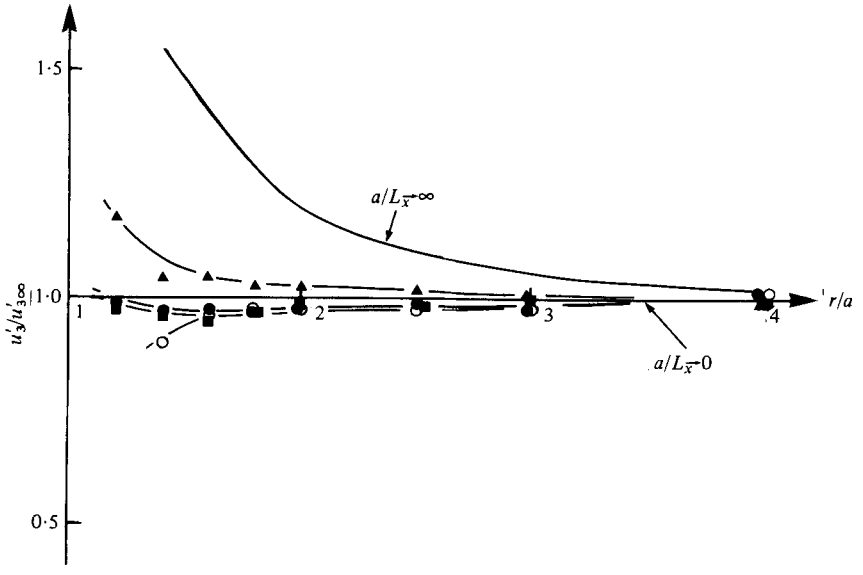

FIGURE 18. Ratio of the local to the upstream values of the r.m.s. axial velocity fluctuations u_3 on the stagnation line $\theta = \pi$ as a function of r/a and a/L_x. Symbols as in figure 15.

5.6. *Behaviour of the axial velocity fluctuations u_3 on $\theta = \pi$*

The ratio of the r.m.s. axial fluctuations u_3' to the upstream value is plotted in figure 18. There is little amplification or reduction except for the smallest scale of turbulence ($a/L_x = 1{\cdot}42$).

This weak change in u_3' is in contradiction to the strong influence of two-dimensional bluff-body distortion on u_3' found by Bearman (1972). Bearman's measurements, over a very limited range of the ratio of body size to L_x, indicated a variation of u_3' which approached the theoretical limits for $a/L_x \to 0$ and $a/L_x \to \infty$. The experiments of Thomas & Hancock (1977) on grid turbulence near a moving wall suggested, as does the present experiment, that u_3' (in their experiment the component parallel to the wall and perpendicular to the mean flow) is not as well predicted as the other two components. The spectra are plotted in figure 19. As with the u_1 component, the low frequency components are reduced when a/L_x is small, but are amplified when a/L_x increases. For $5 \geqslant \hat{\kappa}_1 \gtrsim 1$ the spectrum at $a/L_x = 1{\cdot}42$ is amplified, but for even higher frequencies the spectrum decreases as the cylinder is approached.

5.7. *Probability measurements*

On the stagnation line the flatness factor $F = \overline{u_1^4}/u_1'^4$ was measured. Surprisingly it was found that, as r/a decreased from 4·0 to 1·2, F *increased* from its usual grid-turbulence, and approximately Gaussian, value of 2·9 to about 3·4 for all values of a/L_x.

A likely mechanism for this change in the probability density can be seen by considering the time dependence of the amplification (or reduction) of the velocity $u_1(t)$. The distortion produced by the cylinder increases ω_2' but leaves ω_3' unchanged. It would therefore be expected that the amplification of $u_1(t)$ would depend on the orientation of $\boldsymbol{\omega}(t)$, and would be greatest when $\omega_2/|\boldsymbol{\omega}|$ is close to unity. Similarly, the reduction of $u_1(t)$ caused by the blocking effect of the cylinder would also be expected

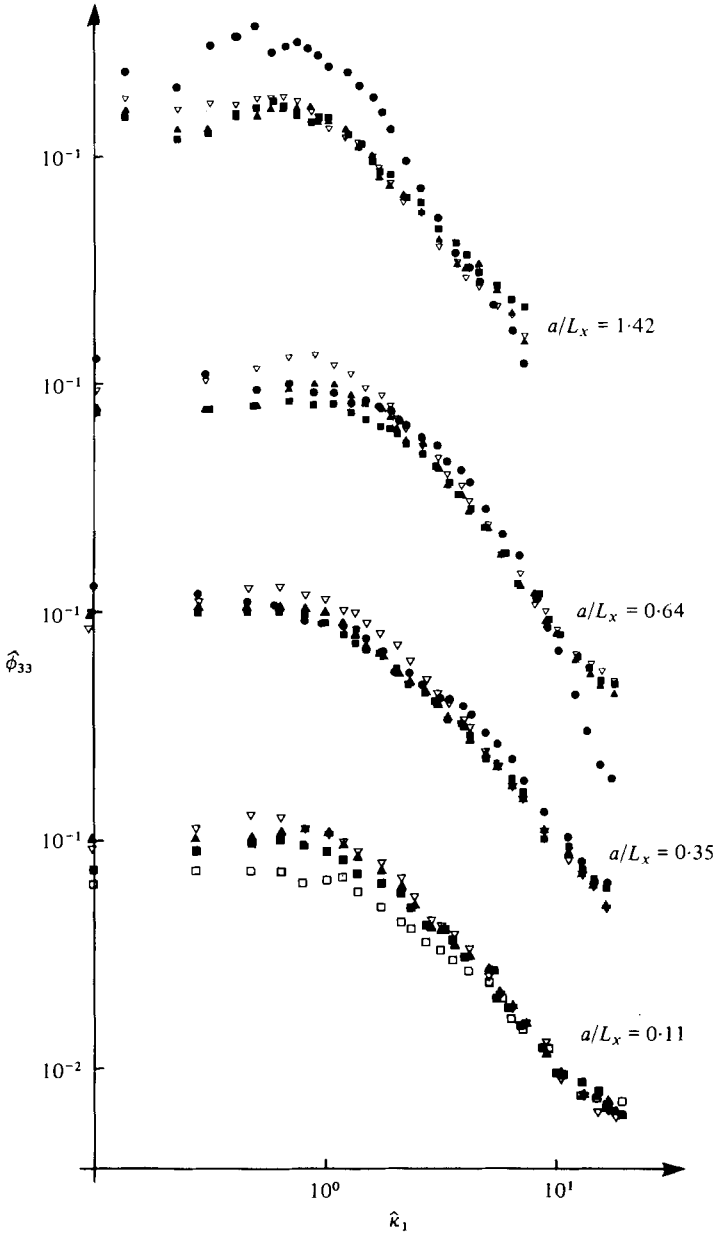

FIGURE 19. Variation of the spectrum of the axial velocity fluctuations u_3 on the stagnation line $\theta = \pi$. Symbols as in figure 16.

to depend on the orientation of $\boldsymbol{\omega}(t)$. In the absence of the cylinder, $u_1(t)$ would be approximately normally distributed, so that the observed probability density of $u_1(t)$ can be considered as a result of the application of a time-dependent amplification (or reduction) to a normally distributed velocity. It can be shown that, with a few weak constraints on the correlation between the orientation of $\boldsymbol{\omega}(t)$ and the magnitude of $u_1(t)$, the resulting probability density has an increased flatness factor.

6. Discussion

6.1. *Physical interpretation of the turbulence distortion*

The salient feature of the experimental investigation of upstream turbulence impinging on a circular cylinder is that the three components of turbulence are amplified or diminished quite differently, sometimes in opposite directions, as either the relative scale of turbulence a/L_x or the position around the cylinder is changed. Broadly, these amplifications or diminutions can be explained qualitatively in terms of the distortion of the turbulent vorticity (either stretching, rotation or 'piling-up') by the mean flow, and in terms of the 'blocking' or the 'source' effect by the surface of the cylinder.

For example, on the stagnation line ω_2' is amplified by the diverging mean streamlines, ω_1' is reduced in proportion to $\overline{U}_1$, and ω_3' remains constant. Therefore for small scales ($a/L_x \gg 1$, or $k \gg 1$), when the source effect is small [$(a/L_x)\,\xi \gg 1$], u_1' increases, u_2' decreases and u_3' increases (by less than u_1'). Close to the surface, where both vorticity distortion and the source effect are significant, the amplification of u_1' decreases, u_2' increases and u_3' continues to increase. For large scales, when $a/L_x \ll 1$ (or $k \ll 1$) the source effect dominates, the turbulence is blocked by the cylinder, and consequently u_1' decreases, u_2' increases and u_3' does not change. These trends are clearly borne out by figures 6, 12 and 18.

The qualitative arguments can also explain the trends in the spectra; see figures 7, 11 and 19. But it can be seen that when $a/L_x \gg 1$, the amplification or reduction due to the vorticity distortion effect is sensitive to the frequency κ_1. When $\kappa_1 \ll 1$ the changes are caused by the stretching or reduction of the vortex lines, but when $\kappa_1 \gg 1$, the vortex lines 'pile up' at the stagnation point as well as being stretched. The piling-up reduces any amplification that may occur (see H, p. 672).

On the centre-line ($\theta = \frac{1}{2}\pi$), ω_1' is greatly amplified by the rotation and stretching of the upstream ω_2 vortex lines, ω_2' is reduced and ω_3' is not changed. Therefore for small scales (when $a/L_x \gg 1$ or $k \gg 1$, and $(a/L_x)\,\xi \gg 1$ or $k\xi \gg 1$) u_2' and u_3' increase and u_1' decreases slightly. Close to the surface (but outside the boundary layer), the amplification of u_2' decreases, and u_3' and u_1' increase. For large scales u_1' increases, u_2' decreases and u_3' does not change. These are the predicted effects and, taking into account the additional velocity fluctuations $u_i^{(w)}$ caused by the wake, these trends are consistent with the measurements shown in figures 10(*a*), (*b*), 11, 15 and 16.

These physical arguments can be and have been used in other flows where turbulence is distorted and impinges on a surface (Bearman 1972; Bradshaw & Wong 1972; Graham 1976).

6.2. *Interaction of the upstream and the wake turbulence*

The measurements of u_2 and of u_1 on $\theta = \frac{1}{2}\pi$ show that, with turbulence intensities $u_{1\infty}'/\overline{U}_\infty$ of about 0·05, the wake-induced velocity fluctuations $u_i^{(w)}$ are comparable with those originating in the upstream turbulence, $u_i^{(T)}$. The results do not enable a clear distinction to be made between these two fluctuations. The problem is analysed in §5.2 and the measurements discussed in §§5.3–5.5. The following conclusions may be made.

(i) The spectrum of $u_i^{(w)}$ may be broadened and amplified by the upstream turbulence; the frequency of the peak may be changed. A small change in end conditions

on the cylinder can have a large effect. $u_i^{(w)}$ and the spectral peak of $u_i^{(w)}$ decrease slowly with r (on $\theta = \frac{1}{2}\pi$), owing to the coherence of the eddies in the x_3 direction. In fact it was observed that $u_1'^{(w)} \propto |r-a|^{-1}$, in agreement with the theoretical variation of the induced velocity outside a Kármán vortex street. This is a much slower decay than the r^{-4} variation found outside a shear layer with less coherent vortices, e.g. a boundary layer (see Phillips 1955).

(ii) Since $u_i^{(w)\prime}/\overline{U}_\infty \ll 1$ at least for $r/a > 1{\cdot}2$ and $\pi \geqslant \theta \geqslant \frac{1}{2}\pi$, it seems likely that $\overline{u_i^{(w)} u_j^{(T)}} = 0$ for any two components of $u_i^{(w)}$ and $u_j^{(T)}$. But $u_i^{(w)\prime}$ definitely varies with $u'_{i\infty}/\overline{U}_\infty$.

(iii) A splitter plate reduces the intensity of vortex shedding, but does not appreciably reduce $u_i^{(w)\prime}$ near the cylinder or wake surface.

(iv) $u_i^{(T)}$ and $u_i^{(w)}$ can only really be distinguished by a more elaborate set of cross-correlation measurements with time delay τ between $u_i(t)$ at a point near the wake, say on $\theta = \frac{1}{2}\pi$, and $u_{\infty i}$ upstream at time $t-\tau$, where τ is the mean travel time between the points. This has yet to be done.

6.3. *Comparison with theory*

By plotting the amplification of the r.m.s. components of turbulence as functions of a/L_x, as in figure 6(*b*), one can obtain an approximate extrapolation of the results to the limits $a/L_x \to 0$ and $a/L_x \to \infty$, where the asymptotic theory of H is applicable. It appears that, as $a/L_x \to 0$, $u_1'/u'_{1\infty}$ tends to the quasi-steady limit, as expected from the theory. But when $a/L_x > 1$, the data for the limited range of a/L_x ($< 1{\cdot}4$) suggest that only when $r-a > L_x$ (e.g. at $r/a = 2{\cdot}0$) does the observed amplification tend to the limit $a/L_x \to \infty$, which was only to be expected, since this is the condition for the validity of the limit. However, when $r-a \ll L_x$ or $(r/a-1)\,a/L_x \ll 1$, such as at $r/a = 1{\cdot}2$, $u_1'/u'_{1\infty}$ should tend to the asymptotic form for $a/L_x \gg 1$ when

$$(r/a-1)\,a/L_x \to 0.$$

Only when $\kappa_1 = 0$ and $\kappa_1 \gg 1$ have the spectra been computed in this limit, but these indicate that on $\theta = \pi$

$$u_1'/u'_{1\infty} \propto (a/L_x)^{\frac{1}{3}}\,(r/a-1)^{-\frac{1}{6}}.$$

Therefore a slow increase with a/L_x is expected until $(a/L_x) > (r/a-1)^{-1}$.

Figure 6(*c*) shows that as $a/L_x \to \infty$ the difference between $\overline{u_1^2}$ and its asymptotic limit is proportional to $(a/L_x)^{\frac{2}{3}}$ as predicted by the theory (see (5.1) and the appendix). On a flat plate parallel to the flow in free-stream turbulence the difference between the variance of the normal component of velocity at a point y above the surface and its asymptotic value as $y/L_x \to 0$ also varies as $(y/L_x)^{\frac{2}{3}}$. In that case the difference is due simply to the reduced surface effect as the scale of turbulence decreases, but in the case of the circular cylinder it is also due to the increase in the effect of vorticity distortion as L_x decreases. The presence of the $\frac{2}{3}$ exponent is a consequence of the Kolmogorov form of the high wavenumber part of the spectrum.

The expansion (5.1) suggests that $u_1'/u'_{1\infty} = 1$ on $\theta = \pi$ at any point r at a value $(a/L_x)_1$ of a/L_x satisfying

$$(a/L_x)^{\frac{2}{3}} \simeq f_1^{-1}\left(\frac{r}{a}\right)\left[1-\left(\frac{u_1'(r)}{u'_{1\infty}}\right)^2\Bigg|_{a/L_x=0}\right]. \tag{6.1}$$

The experimental results of figure 6(*b*) indicate that $(a/L_x)_1 \simeq 0{\cdot}4$ and does not vary significantly over the range $3 > r/a > 1{\cdot}2$. This implies, from (6.1) and the form of $u_1'/u_{1\infty}'|_{a/L_x=0}$, that

$$f_1(r/a) = (a/L_x)^{-\frac{2}{3}}[1-\overline{U}_1^2/\overline{U}_\infty^2] = (a/L_x)_1^{-\frac{2}{3}}[2(r/a)^{-2}-(r/a)^{-4}]. \tag{6.2}$$

If (6.2) is substituted into (5.1), the value of $u_1'/u_{1\infty}'$ on the stagnation line is predicted to within 5% for $a/L_x < 0{\cdot}35$ and to within 10% for $a/L_x < 1{\cdot}42$. This may be a useful semi-empirical result.

The amplification of the r.m.s. values of u_2 on $\theta = \pi$ and $\theta = \frac{1}{2}\pi$ are compared with the theoretical asymptotic limits as $a/L_x \to 0$ and $a/L_x \to \infty$. Comparing figure 12 with figure 6(*a*), we see that, when $a/L_x = 0{\cdot}11$, $u_1'/u_{1\infty}'$ is closer to the asymptotic limit as $a/L_x \to 0$ than $u_2'/u_{2\infty}'$. One possible explanation is that, since the streamwise scale of the lateral fluctuations (L_{x2}) is only one-third of that of the streamwise fluctuations (L_x), the vorticity distortion effect is relatively stronger for the u_2 component.

At $\theta = \frac{1}{2}\pi$ (figure 15), the value of $u_2'/u_{2\infty}'$ when $a/L_x = 0{\cdot}11$ is also further from the large-scale limit. But this may also be due to wake-induced fluctuations.

The comparison between the measured and theoretical ratios $R_{\phi 1}$ and $R_{\phi 2}$ of the local to the upstream velocity spectra for the low and high frequency limits and for large and small scales of turbulence are shown in figures 8, 9, 11(*b*), 14 and 17. Since the theoretical difference between $R_{\phi i}(\kappa_1 \to 0)$ and the asymptotic limit for $R_{\phi i}$ as $a/L_x \to 0$ and $\kappa_1 \to 0$ is proportional to $(a/L_x)^{\frac{5}{3}}$ (appendix), the differences for $a/L_x = 0{\cdot}11$ and $0{\cdot}35$ should be about 3 and 20% if the theory is correct and applicable. The results for ϕ_{11} (figures 8 and 11*b*) are consistent with this estimate, but those for ϕ_{22} are not (figures 14 and 17). The presence of vortex shedding does not explain the low value of ϕ_{22} observed on the stagnation line (figure 14), though it may explain $R_{\phi 2}$ in figure 17 for large and small scales. When $\kappa_1 \to 0$ and $a/L_x \gg 1$, the asymptotic form for $R_{\phi i}$ depends on $(r/a-1)\,a/L_x$. It can be seen in figure 8 that, even when $a/L_x = 5$, $R_{\phi 1}$ approaches the asymptotic form for $a/L_x \gg 1$ and $(r/a-1)\,a/L_x \gg 1$ only when $r/a = 1{\cdot}8$. Consequently when $a/L_x = 1{\cdot}42$, one would not expect the results to approach this limit.

At high frequencies, the effects of vortex shedding and the presence of the surface of the cylinder become negligible compared with vorticity distortion. The theory then predicts that $R_{\phi i}$ becomes a function of $r/a-1$ only. Figure 9 shows that on the stagnation line $R_{\phi 1}$ agrees with the theoretical amplification to within the experimental accuracy. $R_{\phi 2}$ agrees with the theoretical form (which is proportional to $(\overline{U}_1/\overline{U}_\infty)^{\frac{5}{3}}$ when $r/a-1 \to 0$) for $r/a > 1{\cdot}5$ and $\kappa_1 = 3{\cdot}5$ (figure 14). This was to be expected, since the theory is valid only when $(r/a-1)\,\kappa_1 \gg 1$; for smaller values of $r/a-1$ the surface blocking effect amplifies $R_{\phi 2}$. The measured $R_{\phi 2}$ on $\theta = \frac{1}{2}\pi$ when $\kappa_1 \gg 1$ agrees reasonably well with the theory, given the fact that the measured spectra did not have the $-\frac{5}{3}$ form over a significant frequency range (figure 17).

The spectra ϕ_{33} of the u_3 component in figure 19 explain the feeble amplification of $u_3'/u_{3\infty}'$ seen in figure 18. The theory indicates that, when $a/L_x \to 0$, $R_{\phi 3} = 1$, but when $a/L_x \gg 1$, $R_{\phi 3}$ increases. The measurements show that $R_{\phi 3}(\kappa_1 \to 0)$ decreases when $a/L_x < 1$ and increases when $a/L_x > 1$. The former effect is not predicted by the theory and there is no obvious explanation.

Comparing the experimental results with the theory of H shows that the main features of the turbulence distortion are described by the asymptotic theories for

large-scale or small-scale turbulence. These theories give useful *quantitative* results for the spectra when $a/L_x \ll 1$ or $a/L_x \gg 1$ and $\kappa_1 \to 0$, or when $\kappa_1 \gg 1$. The quantitative agreement is best for the streamwise turbulence component. The general theory developed in H does not have to be applied in order to calculate the above limits. These can be obtained from homogeneous rapid-distortion theory for $a/L_x \gg 1$, at least sufficiently far from the cylinder, or quasi-steady potential flow theory for $a/L_x \ll 1$. The computations of the general theory were necessary to show that these asymptotic limits described the main features of the flow. The general theory is also necessary for calculating u_i within an integral scale of the surface even when $a/L_x \gg 1$.

6.4. *Decay of the turbulence*

For the smallest scale of turbulence relative to the cylinder radius ($a/L_x = 1{\cdot}42$), the ratio of the time taken for a fluid particle to travel along the stagnation line from $r/a = 4{\cdot}0$ to $r/a = 1{\cdot}2$ to the Lagrangian or turnover time scale L_x/u' was

$$(4a/U)(L_x/u') \simeq 0{\cdot}3.$$

The decay of the grid turbulence in this time is less than 10%. Therefore for the energy-containing eddies, it would be expected that dissipation and nonlinear effects are small compared with the effects of vorticity distortion and 'blocking' by the surface (H, §§5.3 and 6.4). However, it was observed that at the highest frequencies at which ϕ_{ii} was measured there was a sharp attenuation of the spectrum. This occurred for $\hat{\kappa}_1 > 15$, 10 and 4 for $a/L_x = 0{\cdot}35$, $0{\cdot}64$ and $1{\cdot}42$ on the stagnation line. A similar effect was observed by Sadeh *et al.* (1970), by Bearman (1972) and by Elliott (1976).

An attenuation of the spectrum at high frequencies was predicted in H [equations (6.52) and (5.52)] on the basis of a linear analysis. Unfortunately there was a mistake in the derivation of the result from the order-of-magnitude estimates of the terms in the vorticity equation. The correct criterion when $\kappa_1 \gg 1$ is that, for viscous effects to be much smaller than the vortex stretching,

$$|Re^{-1}\,\partial^2\omega_2/\partial x_1^2| \ll |\omega_2\,\partial\overline{U}_2/\partial x_2|,$$

which implies that, since $\omega_2 \propto (2\xi)^{-1}\exp[-i(\frac{1}{2}\kappa_1)\log_e\xi]$,

$$\xi \ll 8^{-\frac{1}{2}}\kappa_1 Re^{-\frac{1}{2}} \quad \text{where} \quad \xi = r/a - 1. \tag{6.3}$$

For the present experiment, this criterion will be violated at $r/a = 1{\cdot}2$ if $\kappa_1 \gg 50$. It seems, therefore, that viscous effects are not the direct cause of the observed decay.

The decay is more probably due to the nonlinear interaction, which, relative to the vorticity distortion effects, increases as κ_1 increases. Typically, on the stagnation line

$$\frac{(\mathbf{u}.\nabla)\boldsymbol{\omega}}{(\boldsymbol{\omega}.\nabla)\mathbf{U}} \sim \frac{\kappa_1\xi^{-2}u'_\infty}{2\xi^{-1}\overline{U}_\infty/a}. \tag{6.4}$$†

With $u'_\infty/\overline{U}_\infty = 0{\cdot}05$ at $\xi = 0{\cdot}2$ the nonlinear effects would be expected to become appreciable for values of κ_1 ($\equiv \hat{\kappa}_1 a/L_x$) of about 4, and would tend to dominate with increasing κ_1 until viscous effects become significant. In terms of the development of

† In H (p. 661), $(\mathbf{u}.\nabla)\boldsymbol{\omega}$ was estimated as $\omega'_\infty u'_\infty/l$; for high frequencies (6.4) is probably a better estimate.

$\phi_{11}(\kappa_1)$ with increasing x_1 (decreasing ξ) the implication is that, for this range of κ_1, the rate at which $\phi_{11}(\kappa_1)$ can be changed by nonlinear effects exceeds the rate at which it is being changed by the distortion. Consequently the value of $\partial\phi_{11}(\kappa_1)/\partial x_1$ would change when κ_1 exceeded the value indicated by 6.4, and this would in turn alter the slope of the spectrum at this frequency. The estimated value of κ_1 is in reasonable agreement with the measurements presented in figure 7.

These results, and those obtained by Elliott (1976) for the spectrum of wake turbulence subjected to a plane strain, are consistent with the notion that a straining distortion can *inhibit* the mechanism of inertial transfer to higher wavenumbers.

R.E.B. and J.C.M. were supported by grants from the Science Research Council. We are grateful for valuable technical assistance from D. Cheesley and D. Lipman in the laboratory of D.A.M.T.P., and from B. Wootton and L. Freeman in the Control Engineering Department, and for computing assistance from Mr Julian Smith. J.C.R.H. is grateful to the Department of Geosciences, North Carolina State University and the Environmental Protection Agency (Grant R804653) for support while this paper was written. The authors wish to acknowledge the constructive criticisms of the referees.

Appendix. Expansion of $\overline{u_i^2}$ and ϕ_{11} ($\kappa_1 = 0$) as asymptotic series when $a/L_x \to 0$†

It is shown in equation (6.10) of H that, given isotropic upstream turbulence with a von Kármán spectrum, the normalized one-dimensional spectrum ϕ_{11} at a point $\mathbf{x}$ of, say, the u_1 component can be expressed in terms of the tensor $M_{in}(\boldsymbol{\kappa}, \mathbf{x})$ which connects the Fourier transform, at wavenumber $\boldsymbol{\kappa}$, of the turbulent velocity components near the cylinder to those upstream:

$$\phi_{11}(\kappa_1 = 0, \mathbf{x}) = \int_{-\infty}^{\infty}\int_{-\infty}^{\infty} \frac{c_3 M_{1n}(\boldsymbol{\kappa}, \mathbf{x})\, M^*_{1m}(\boldsymbol{\kappa}, \mathbf{x})\,(k^2\delta_{nm} - \kappa_n\kappa_m)\, d\kappa_2\, d\kappa_3}{[g_2(a/L_x)^2 + k^2]^{\frac{17}{6}}}. \quad \text{(A 1)}$$

Here

$$c_3 = (55/36\pi)\, 0{\cdot}1955(a/L_x)^{\frac{2}{3}} = g_3(a/L_x)^{\frac{2}{3}}, \quad g_2 = 0{\cdot}558,$$

and $k = |\boldsymbol{\kappa}|$. In the limit $\boldsymbol{\kappa} \to 0$, M_{in} was shown to have a power-series expansion of the form

$$M_{in}(\boldsymbol{\kappa}, \mathbf{x}) = M^{(0)}_{in} + i\kappa_j M^{(1)}_{in,j} + \kappa_j\kappa_k \ln|\kappa_3|\, M^{(L)}_{in,jk} + \kappa_j\kappa_k M^{(2)}_{in,jk} + \ldots, \quad \text{(A 2)}$$

where $M^{(0)}_{in}$, $M^{(1)}_{in}$, etc., are functions of $\mathbf{x}$.

By computation and asymptotic analysis it was shown in H that M_{in} is bounded at a given $\mathbf{x}$ for all values of $\boldsymbol{\kappa}$ satisfying $0 < |\boldsymbol{\kappa}| < \infty$. Typically $|M_{in}|$ is less than 10 except very close (less than 0·1 radii) to the body.

If (κ_2, κ_3) are expressed as $(\bar{k}\cos\phi, \bar{k}\sin\phi)$, then (A 1) can be rewritten as

$$\phi_{11}(\kappa_1 = 0, \mathbf{x}) = g_3(a/L_x)^{\frac{2}{3}} \int_0^{\infty}\int_0^{2\pi} \frac{\bar{k}^3 F(\bar{k}, \phi)\, d\phi\, d\bar{k}}{\{g_2(a/L_x)^2 + \bar{k}^2\}^{\frac{17}{6}}}, \quad \text{(A 3)}$$

where

$$F(\bar{k}, \phi) = \{M_{1n} M^*_{1m}(k^2\delta_{nm} - \kappa_n\kappa_m)/\bar{k}^2\} \quad \text{when} \quad \kappa_1 = 0. \quad \text{(A 4)}$$

† The nomenclature is the same as in H except that $\hat{\phi}_{11}$ replaces $\hat{\Theta}_{11}$.

It follows from the expansion (A 2) of M_{in} when $\kappa \to 0$ that we can express the first integral in (A 4) as

$$\int_0^{2\pi} F\,d\phi = \lambda^{(0)}(\mathbf{x}) + \Delta F(\bar{k}, \mathbf{x}), \tag{A 5}$$

where $\lambda^{(0)}(\mathbf{x})$ is the limit as $\kappa \to 0$ and

$$\Delta F = \bar{k}^2 \ln|\bar{k}|\, \lambda^{(L)} + \bar{k}^2 \lambda^{(2)} + \ldots \quad \text{as} \quad \kappa \to 0, \tag{A 6}$$

but $\Delta F = O(1)$ when $\bar{k}$ is $O(1)$.

Thus (A 4) becomes

$$\phi_{11}(\kappa_1 = 0, \mathbf{x}) = \phi_{11}^{(0)}(\mathbf{x}) + g_3 (a/L_x)^{\frac{2}{3}} I(\mathbf{x}),$$

where

$$I(\mathbf{x}) = \int_0^\infty \frac{\bar{k}^3 \Delta F(\bar{k}, \mathbf{x})\, d\bar{k}}{[g_2 (a/L_x)^2 + \bar{k}^2]^{\frac{17}{6}}}. \tag{A 7}$$

In the limit $a/L_x \to 0$, asymptotic expansions can be used to find the form of $I(x)$, by using the properties of $\Delta F(\mathbf{k}, \mathbf{x})$ stated in (A 6). We find that as $a/L_x \to 0$

$$I(\mathbf{x}) = I^{(0)}(\mathbf{x}) + (a/L_x)^{\frac{1}{3}} \ln(a/L_x)\, g_4 \lambda^{(L)} + O((a/L_x)^{\frac{1}{3}}), \tag{A 8}$$

where

$$I^{(0)}(\mathbf{x}) = \int_0^\infty \frac{\Delta F(\bar{k}, \mathbf{x})\, d\bar{k}}{\bar{k}^{\frac{8}{3}}},$$

$$g_4 = (\tfrac{6}{11} g_2^2 - \tfrac{12}{5} g_2) = -1{\cdot}17.$$

To evaluate $I^{(0)}(\mathbf{x})$, ΔF is required over the entire range of $\bar{k}$. The computations in H were not sufficiently extensive to provide this information, but they showed that ΔF is $O(1)$ when $\bar{k}$ is $O(1)$. Consequently $I^{(0)}$ and $I(\mathbf{x})$ are $O(1)$ when $a/L_x \to 0$. Thence we conclude that

$$\phi_{11}(\kappa_1 \to 0, \mathbf{x}) = \phi_{11}^{(0)}(\kappa_1 \to 0, \mathbf{x}) + O((a/L_x)^{\frac{2}{3}}).$$

Alternatively, if ϕ_{11} is normalized on L_x as in (3.3), then

$$\hat{\phi}_{11}(\hat{\kappa}_1 \to 0, \mathbf{x}) = \hat{\phi}_{11}^{(0)}(\hat{\kappa}_1 \to 0, \mathbf{x}) + g_3 (a/L_x)^{\frac{5}{3}} I^{(0)}(\mathbf{x}) + O((a/L_x)^2 \ln(a/L_x)). \tag{A 9}$$

A similar analysis also based on the properties of M_{in} shows that

$$\overline{u_1^2} = \overline{u_1^2}(a/L_x \to 0, \mathbf{x}) + O((a/L_x)^{\frac{2}{3}}), \tag{A 10}$$

the next-order term being $O((a/L_x)\ln(a/L_x))$.

REFERENCES

Batchelor, G. K. 1960 *The Theory of Homogeneous Turbulence.* Cambridge University Press.

Bearman, P. W. 1968 The flow around a circular cylinder in the critical Reynolds number regime. *Nat. Phys. Lab. Aero. Rep.* no. 1257.

Bearman, P. W. 1972 Some measurements of the distortion of turbulence approaching a two-dimensional body. *J. Fluid Mech.* **53**, 451.

Bradshaw, P. & Wong, F. Y. F. 1972 The reattachment and relaxation of a turbulent shear layer. *J. Fluid Mech.* **52**, 113.

Britter, R., Hunt, J. C. R. & Puttock, J. 1976 Predicting pollution concentrations near buildings and hills. *Conf. Systems & Models in Air & Water Pollution. Inst. Meas. Control, London.*

Comte-Bellot, G. & Corrsin, S. 1971 Simple Eulerian time correlations of full- and narrow-band velocity signals in grid-generated 'isotropic' turbulence. *J. Fluid Mech.* **48**, 273.

ELLIOTT, C. J. 1976 Eddy structure in turbulent flow. Ph.D. thesis, University of Cambridge.

GERRARD, J. H. 1965 A disturbance-sensitive Reynolds number range of the flow past a circular cylinder. *J. Fluid Mech.* **22**, 187–196.

GRAHAM, J. M. R. 1976 Turbulent flow past a porous flat plate. *J. Fluid Mech.* **73**, 565.

GUTMARK, E., WOLFSHTEIN, M. & WYGNANSKI, I. 1978 The plane turbulent impinging jet. *J. Fluid Mech.* **88**, 737.

HUNT, J. C. R. 1971 The effect of single buildings and structures. *Phil. Trans. Roy. Soc.* A **269**, 457.

HUNT, J. C. R. 1973 A theory of turbulent flow around two-dimensional bluff bodies. *J. Fluid Mech.* **61**, 625.

HUNT, J. C. R. 1976 Turbulent velocities near and fluctuating surface pressures on structures in turbulent flows. *Proc. 4th Int. Conf. Wind Effects on Buildings & Structures*, p. 309. Cambridge University Press.

HUNT, J. C. R. & GRAHAM, J. M. R. 1977 Free-stream turbulence near plane boundaries. *J. Fluid Mech.* **84**, 209.

JACKSON, R., GRAHAM, J. M. R. & MAULL, D. J. 1973 The lift on a wing in turbulent flow. *Aero. Quart.* **24**, 155.

MIYAZAKI, H. & SPARROW, E. M. 1976 Potential flow solution for cross flow impingement of a slot jet on a circular cylinder. *Trans. A.S.M.E., J. Fluid Engng* **98**, 249.

PARKINSON, G. V. & JANDALI, T. 1970 A wake source model for bluff body potential flow. *J. Fluid Mech.* **40**, 577–594.

PETTY, D. G. 1972 Discussion contribution. *IAHR/IUTAM Conf. Flow Induced Vib., Karlsruhe.*

PHILLIPS, O. M. 1955 The irrotational motion outside a free boundary layer. *Proc. Camb. Phil. Soc.* **51**, 220.

SADEH, W. Z., SUTERA, S. P. & MAEDER, P. F. 1970 An investigation of vorticity amplification in stagnation flow. *Z. angew. Math. Phys.* **21**, 717.

THOMAS, N. H. & HANCOCK, P. 1977 Grid turbulence near a moving wall. *J. Fluid Mech.* **82** 481–496.

TOWNSEND, A. A. 1976 *The Structure of Turbulent Shear Flow*, 2nd edn. Cambridge University Press.

TUCKER, H. S. & REYNOLDS, A. J. 1968 The distortion of turbulence by irrotational plane strain. *J. Fluid Mech.* **32**, 657.

VICKERY, B. J. 1966 Fluctuating lift and drag on a long cylinder of square cross-section in a smooth and in a turbulent stream. *J. Fluid Mech.* **25**, 481.